SIMULATION STUDIES IN UNCONVENTIONAL GAS RESERVOIRS

by

Swapnil Vijaykumar Thakur

A thesis submitted to the faculty of
The University of Utah
in partial fulfillment of the requirements for the degree of

Master of Science

Department of Chemical Engineering

The University of Utah

May 2011

The University of Utah Graduate School

STATEMENT OF THESIS APPROVAL

The thesis of **Swapnil Vijaykumar Thakur**

has been approved by the following supervisory committee members:

Milind D. Deo	, Chair	**12/21/2010** Date Approved
John McLennan	, Member	**12/21/2010** Date Approved
Peter Rose	, Member	**12/21/2010** Date Approved

and by **JoAnn S. Lighty** , Chair of the Department of **Chemical Engineering**

and by Charles A. Wight, Dean of The Graduate School.

ABSTRACT

Producing gas from unconventional sources is critical for developing secure sources of energy. In unconventional gas reservoirs like in tight gas sands the permeability values are extremely low. In such cases the natural fractures and fracture networks play an important role in enhancing the production rate by increasing permeability. This thesis describes an approach of representing the fracture network and then analyzing the effect of the fracture network on production predictions. The first stage of this process is representing the fracture network as a discrete fracture network. The created discrete fracture network is then introduced into a geomechanical simulator. The geomechanical simulator is used to create a complex hydraulic fracture in the presence of the existing natural fractures. This system of complex fractures is incorporated into a flow simulator for predicting the production rates and to generate pressure signatures. This study includes studying the effect of different fracture orientation, fracture spacing on the production values. There is a possibility that fracture maybe of irregular shape and may not intersect with the well or with other conductive fractures, but may show conductive features due to the geomechanical stress and strains applied on them at reservoir condition. The simulation results for tight gas sands obtained from geomechanical simulation coupled with fluid flow are highlighted and discussed.

CONTENTS

LIST OF FIGURES

LIST OF TABLES

NOTATIONS AND SYMBOLS

STC: Stock tank condition

Φ Porosity

k: Permeability

μ: Viscosity

k_{rl}: Relative Permeability

V: Volume

P: Pressure

F: Force

A: Area

E: Young's Modulus

ϒ Permeability Modulus

ν Poisson Ratio

q: Production or Injection of Fluid

σ_1: Maximum Principal Stress

σ_2: Intermediate Principal Stress

σ_3: Minimum Principal Stress

ACKNOWLEDGEMENTS

First and foremost, I am grateful to my mentors Dr. Milind Deo and Dr. John McLennan for their guidance and support provided for my research. They were always approachable and their suggestions and recommendations have immensely helped me in thesis preparation.

Next, I would also like to thank Dr. Peter Rose for being a part of my thesis examination committee. I would also like to thank RPSEA for project funding and providing me the opportunity. I also acknowledge ITASCA and their team for providing their software and guidance. I also thank Dr. Ravi Bhide for his support.

I would like to thank all the faculty and staff of the Chemical Engineering Department.

Last but not least, I am grateful to all my friends and members of PERC for giving necessary support and keeping a cheerful ambience in laboratory.

CHAPTER 1

INTRODUCTION

Unconventional gas reservoir is a term commonly used to refer to a low permeability reservoir that produces mainly dry natural gas. Mostly the low permeability reservoirs developed are sandstone, but significant quantities of gas can also be produced from low-permeability carbonates, shales, and coalbed methane. Normally, large hydraulic fracture treatments with multiple stages are used to achieve this stimulation. In most naturally fractured unconventional gas reservoirs, horizontal wells can be drilled. Even under this condition stimulation through hydraulic fracturing is still practiced.

The optimization of any unconventional gas reservoir is extremely important. We have to consider the geotechnical and engineering aspects to find out the optimized number of wells to be drilled and their location, as well as the drilling and completion procedures for each well. In order to do this comprehensive data are required to understand the complexity of reservoir and to develop the recovery techniques. Due to the low porosity and low permeability of this typical reservoir the resources required to understand and develop are higher than those involved in conventional reservoir.

An unconventional gas reservoir produces comparatively less gas and takes a longer time than a conventional gas reservoir. In order to get good recovery more wells

with smaller well spacing must be drilled and hydraulic fracturing must be done in an unconventional gas reservoir to recover a large percentage of the original gas in place.

In a conventional reservoir connectivity may be more than in an unconventional gas reservoir. The other factors which hinder the recovery in unconventional gas reservoirs are the orientation of fractures, the distance between the fractures, the azimuth of the fractures, the geometry and size of the reservoir, etc. All of these factors can be studied using simulation technique before the hydraulic fracturing is done. This helps in efficient drilling, giving best recovery of the gas from the unconventional gas reservoir.

Unconventional gas reservoirs comprises mainly of following generic types:-

Tight Gas

Shale Gas

Coalbed Methane

1.1 Tight gas reservoirs

Tight gas is natural gas which is difficult to access because of the nature of the rock surrounding the deposit. The cost to recover the gas from tight gas sands is very high because it is extremely difficult to recover than the conventional natural gas. Normally, natural gas is easy to recover because it occurs in porous rock, i.e., better porosity and permeability. This is not the case in tight gas sands as the sandstone, shale, or other rocks are less permeable. The lack of permeability locks the tight gas up underground, which makes the recovery an expensive affair. As the demand for natural gas has grown, attempts have been made to recover gas from tight gas deposits. While tight gas is costly to extract, high gas prices can be used to justify this high cost operation. Most tight gas deposits date to the Paleozoic era, which means that these

deposits are at least 251 million years old. The advanced age of such deposits is presumably responsible for their inaccessibility. These deposits can also be much deeper than ordinary gas deposits, posing additional challenges. Companies which work with tight gas are required to use a variety of survey tactics to identify potential sources of gas, and to target the best spots for drilling.

1.2 Coalbed methane

Coalbed methane (CBM) is simply methane found in coal seams. CBM is generated either from a biological process, as a result of microbial action, or from a thermal process, as a result of increasing heat with depth of the coal. Often a coal seam is saturated with water, with methane adsorbed in the coal. As the methane is adsorbed on coal, a technique of adsorption- desorption is generally used for the recovering the gas.

1.3 Shale gas

Shale gas is defined as natural gas from shale formations. The shale acts as both the source and the reservoir for the natural gas. Older shale gas wells were vertical while more recent wells are primarily horizontal and need artificial stimulation, like hydraulic fracturing, to produce. The most significant trend in US natural gas production is the rapid rise in production from shale formations. In large measure this is attributable to significant advances in the use of horizontal drilling and well stimulation technologies and refinement in the cost-effectiveness of these technologies. Hydraulic fracturing is the most significant of these.

1.4 Motivation

The discrete fracture network found in the rocks is complex and not well connected and hence requires special stimulation technique like hydraulic fracturing. To do the hydraulic fracturing, an intuitive guess of where to fracture has to be done. This can be better achieved if we do the simulation studies for the fracture networks. Also there are certain parameters which can dictate the direction and the rate of the flow of the gas in a particular reservoir. The geomechanical impact of reservoir rock on the flow if studied will help us in making the guess of where the hydraulic fracturing should be done for most efficient and economical recovery.

To study all these criteria simulation work needs to be done. The simulation studies will help in predicting the recovery of gas. They also help us to find out the effect of hydraulic fracturing on the recovery of gas. A parametric sensitivity study helps us to find out how the reservoir properties and fracture network affect the flow of fluid. To study these parameters series of simulations are carried out. A fluid flow simulation study was done using the UFES simulator to see the effect of hydraulic fracturing. For parametric and sensitivity study a commercial simulator 3DEC was used.

CHAPTER 2

LITERATURE SURVEY

2.1 Introduction

It was assumed that horizontal fluid flow had no gravity effect and an isothermal single phase fluid with purely elastic rock properties, i.e., the changes occurring due to the stress change, are reversible and hence geomechanics was ignored in reservoir simulators. When the pressure and properties changes are small this assumption can be justified. But this is not necessarily the case in tight gas sands as the stresses are large. This brings in the need of a new reservoir simulator where the stress-dependent properties are considered. Due to the dependence of permeability on the pressure changes there was a need to develop a reservoir simulator which can handle the changes occurring in permeability due to stress. In the reservoir, effective stress is increased with withdrawal of the fluid, and this leads to a decrease in pore pressure. Since the overburden force on the reservoir rock remains the same, the decreasing pore pressure results in an increased effective stress, which can reduce permeability.

With this the several approaches are made to couple the reservoir simulation with the geomechanics. This coupling between the reservoir and deformation can be made in various forms (Samier et al., 2003). The main approaches are

Fully Coupled Approach

Iterative Coupled Approach

2.1.1 Explicitly Coupled Approach

Among all of these, the fully coupled approach is the tightest coupling approach since the reservoir pressure and temperature and deformations are solved simultaneously. The solution obtained from this approach is more accurate in comparison to other approaches. The major pitfall with this approach is that it is extremely time consuming since it requires solving for flow variables (such as pressure, saturation, compositions) and for geomechanics variables (such as stresses, strains) simultaneously. Thus solving of large problem using this approach is extremely expensive computationally.

2.1.2 Iterative Coupled Approach

In an iterative coupled approach, the coupling is less rigorous. The geomechanics calculations are not performed at the same time as the reservoir fluid calculations. One calculation is done at a time and the information obtained from the geomechanics module is exchanged with the reservoir module back and forth. Thus the reservoir model is affected by the geomechanics model. The main advantage of this approach over the fully coupled approach is that coupling between a reservoir simulator and a geomechanics module could be implemented without making many changes to either code.

In an iterative coupled scheme, pressure can be solved by a conventional simulator that is modified to generate porosity and from this the calculated reservoir porosity is provided to a geomechanical simulator to calculate displacements. Also in this

approach two different calculation approaches can be used. A fluid flow simulator can use the volume based grid whereas the geomechanics can be a finite element node based simulator.

An explicit coupling method is a special case of the iterative coupled approach. In this approach the information is taken from a reservoir simulator and sent to a geomechanics module but the values from geomechanics simulator are not fed back to the reservoir simulator. Thus in this approach the reservoir flow is not at all affected by the geomechanical response calculated in geomechanics module.

2.1.3 Geomechanics Effects on Porosity

The porosity φ^* can be treated as an intermediate unknown, and it is a function of the reservoir porosity φ, and the volumetric strain ε_v. This relation can be used to transfer the information from the geomechanics equations to the reservoir flow equations. On the other hand, fluid pressure can be used for transfer of the information from the reservoir flow equations to the geomechanics equations. In the most general case there is two-way coupling or feedback between fluid flow and geomechanics solutions. In one class of restricted coupling, the porosity φ^* is computed solely as a function of pressure and temperature but not volumetric strain. This may occur in a conventional reservoir simulator where fluid flow is solved in reservoir simulator. The values obtained from this simulation are then passed on to a geomechanics module. In this case the coupling will be "one-way" since the fluid flow calculations are independent of the geomechanical responses. The one-way coupled approach is also called explicitly coupled approach. (D Tran, 2005)

2.1.4 Geomechanical Effects on Permeability

Changes in permeability with stress and strain can be measured in the laboratory. The change in permeability can be modeled in several different ways, which are described below.

Function of Porosity: The permeability is expressed as a function of porosity, so the permeability tensor, k, is an indirect function of geomechanical responses since reservoir porosity is function of porosity and effective strain, and permeability is function of reservoir porosity. We can see the relation in following equation.

$$\phi^{*} = \phi^{*}(\phi, \varepsilon v)$$

and

$$k = k(\phi^{*})$$

Function of volumetric strain or mean effective stress: The absolute permeability can be expressed as a direct function of volumetric strain, volumetric strain and temperature, or mean effective stress (D Tran, 2005)

2.2 Fractured reservoir rock mechanics

A fractured reservoir is a rock mass built from zones or blocks of intact rock bounded by mechanical discontinuities with limited shear and tensile strength. The discontinuities have usually been created and activated by changes in the in-situ stress/strain field which caused the failure criteria for parts of the rock mass to be exceeded, or by a combination of changes in stress/strain and pore fluid chemistry.

Mechanical discontinuities which make a steep angle to the bedding plane are classified as joints and fractures.

Joints: In joints there is no natural shear displacement, usually no significant aperture, and minimal control on fluid flow at depth.

Fractures: In fractures there is limited natural shear displacement, of order of 1 mm, which may have dilated the fracture to create an aperture and so have relatively high permeability and storage capacity. There is detectable control on fluid flow; therefore, a fracture is both a mechanical and a hydraulic discontinuity.

At a larger scale, faults have natural shear displacements from centimeters to kilometers and can act either as permeability barriers or conduits for flow. Like fractures, a fault is both a mechanical and hydraulic discontinuity.

All these discontinuities have distinct geometries with local and regional trends controlled by the stress/strain field which overloaded the rock mass to create them. If the process of creation produces dilation, for example, because the normal stress acting across the discontinuity is low in relation to the strength of the surface topography, then apertures will be created along the line of the discontinuity, producing a high permeability fracture flow network surrounding blocks of intact rock. These apertures may be enhanced by dissolution at any time. This is the conventional conceptual model of a fractured reservoir used by reservoir engineers.

Reducing the pore pressure in the reservoir further increases the effective stress and cause the rock mass that is the reservoir to strain. The strain field generated will not only change the permeability of the intact rock and the fractures, but by altering pore throat geometry, will also affect the capillary entry pressures and hence the balance

between the viscous and capillary forces that control the exchange of fluids between the intact rock and the fractures (Lorenz, 1999).

2.3 Intact rock permeability and pore geometry sensitivity to stress

It is normally assumed that the stress-state at any point in the reservoir is defined by three mutually orthogonal normal total principal stresses σ_1, σ_2 and σ_3, with σ_3 normally being subhorizontal at depths beyond about 1000 m. Production by depletion will increase the effective stresses, i.e., the component of total stress which causes strain, in the reservoir rock according to Biot's equation (Longmoure, 2002):

$$\text{Effective Stress (e.g., } \sigma 1') = \text{Total Stress } (\sigma 1) - \text{Biot's Constant} \times \text{Pore Pressure}$$

2.4 UFES simulator

The governing equations of the black-oil model are basically the continuity or the mass- conservation equations. Both the single- and multiphase flow equations are discussed in this section (Yang, 2003).

2.4.1 Single-phase flow

The continuity equation for the single-phase, subsurface flow problem can be derived from the general continuity equations by including porosity Φ in the accumulation term

$$-\nabla.\rho v = \frac{\partial(\phi\rho)}{\partial t} + q \tag{2.1}$$

where q is the mass injected or produced per unit bulk volume per unit time. Dividing Equation (2.1) by the fluid density at Stock Tank condition (STC), ρSTC, yields

$$-\nabla.\frac{\rho}{\rho_{stc}} * v = \frac{\partial(\phi\frac{\rho}{\rho_{stc}})}{\partial t} + \frac{q}{\rho_{stc}} \tag{2.2}$$

$$-\nabla.\frac{v}{B} = \frac{\partial(\phi\frac{S_l}{B_l})}{\partial t} + \frac{q_l}{} \tag{2.3}$$

where q_l is the volume injected or produced per unit bulk volume per unit time at stock-tank conditions.

2.4.2 Multiphase flow

Subscript ‘l’ is added to represent different phases to extend Equation (2.4) to multiphase flow. The change of phase saturation, S_l is added.

$$-\nabla.\frac{v}{B} = \frac{\partial(\phi\frac{S_l}{B_l})}{\partial t} + \frac{q_l}{} \tag{2.4}$$

From definition of relative permeability we know

$$-\nabla.\frac{k.k_{rl}}{B_l\mu_l}\nabla\varphi_l = \frac{\partial(\phi\frac{S_l}{B_l})}{\partial t} + q_l \tag{2.5}$$

Writing the above equation for Gas- water system we get;

For Gas

$$-\nabla.\frac{k.k_{rg}}{B_g\mu_g}\nabla\varphi_l = \frac{\partial(\phi\frac{S_g}{B_g})}{\partial t} + q_g \tag{2.6}$$

For water

$$-\nabla.\frac{k.k_{rw}}{B_w\mu_w}\nabla\varphi_l = \frac{\partial(\phi\frac{S_w}{Bw})}{\partial t} + q_w \tag{2.7}$$

In the University of Utah's UFES simulator this problem is solved by finite-difference discretization of the differential equations. To solve the equations for complex fractured systems, finite element method is implemented (Yang, 2003).

CHAPTER 3

INTRODUCTION TO 3DEC SIMULATOR

3.1 Introduction to 3DEC

Rock stresses are measured at a local point in space and determination of the state of stress in large rock masses is affected by heterogeneity and the stress field is disturbed by fractures and boundaries. The use of numerical techniques is done to model the heterogeneities in rock mass. The 3DEC distinct element method is mainly used to model three-dimensional (3D) structural problems (Itasca, 2009).

The distinct element method is implemented in the computer program 3DEC and its applicability in field of rock mechanics is helpful for solving reservoir engineering problems where both flow and stress need to be considered. This can be used to model 3D stress fields in gas reservoirs. The fluid flow capability of this software can be coupled and used to find out the associated geomechanical stresses, as well as the fluid migration, accumulation in the reservoir.

The 3-D distinct element code used to perform numerical experiments and simulate the coupled hydromechanical behavior of a fractured rock mass subjected to mechanical stress and hydraulic pressure boundary conditions. In the version of 3DEC used, flow of fluid only occurs in fractures and matrix flow is not possible.

3.1.1 Distinct element code for discontinuous modeling

In the distinct element method, a block can be represented as an assembly of discrete blocks. The blocks are connected by joints or faults and act like an interface between the distinct bodies. The contact forces and displacements at the interfaces of a stressed assembly of block are computed and this calculation also traces the movement of the blocks. The deformable blocks or rigid blocks are connected by spring like joints. These joints have normal and shear stiffness, respectively. The unknowns in this calculation are nodal displacements and rotations of the blocks. The solution scheme used by this distinct element code is explicit time marching and finite contact stiffness. Block displacements are calculated from out of balance moment and forces applied to the center of gravity of each block. The resultant forces include the boundary forces applied to the edges of the block and gravity. The calculation steps are cycled until an equilibrium mechanical state or a continuing failure is reached for the blocks.

We will assume that the matrix permeability is almost negligible and there is no significant fluid flow in the matrix. Also, Itasca's 3DEC does not have that facility yet. With this assumption, flow is possible only in the fracture. The fractures were extensively studied, because of their influence on the overall mechanical and hydraulic behavior of rock masses.

In the distinct element code, a joint is treated like a fracture which is an interface between two rock surfaces, and the hydromechanical behavior of the joint is controlled primarily by the roughness of the two surfaces. Roughness is a function of the genesis of the joint. Tensile fractures, for example, have a more pronounced roughness than fractures that have experienced some shear deformation.

The fractures in the rock exhibit significantly different hydro-mechanical behavior from the entire rock considered. Also the deformability of fractures is therefore higher than the bulk or the intact blocks. The shear strength of the fractures is different from the rock itself. Most of the gas is stored in the pores inside the matrix and it is not always that all the fractures are connected. Hydraulic fracturing is done to improve the connectivity of the fractures and recover the gas at faster pace. Thus, in spite of having good volume of gas in the reservoir we are unable to recover the gas efficiently. In order to optimize the recovery, the discrete fracture network and its orientation need to be studied. This study helps in understanding the nature of the flow and hence can lead to more efficient and economical recovery of tight gas.

3.2 Flow in a discrete fracture network

In 3DEC, the fluid flow is calculated using the Navier-Stokes equation. When the Navier-Stokes equation for fluid flow between two almost parallel, impermeable boundaries is combined with the condition of incompressibility of the fluid, it simplifies to the Reynolds equation

$$(\frac{\mathrm{u}^3 \rho g}{12\mu} * \Phi, i)_{,i} = 0 \tag{3.1}$$

where: $u\ (x_i)$ is the distance between the impermeable boundaries at some point x_i (i = 1, 2) in the plane (the Navier-Stokes equation is integrated over the distance between the impermeable boundaries);

$\Phi = z+p/\rho g$ is the hydraulic head;

g is the acceleration due to gravity;

ρ is the fluid density;

μ is the fluid viscosity;

Z is the elevation; and

P is the pressure in the fluid.

The above equation is valid as long as inequality Eq. (3.2) is satisfied — i.e.,

$$\alpha \rho u_c \frac{v_{\max}}{\mu} << 1 \tag{3.2}$$

α is the angle between the two surfaces enclosing the fluid;

u_c is the characteristic cross-sectional dimension; and

v_{max} is the maximum velocity of the fluid.

The fluid flow rate per unit width of the plates may be written as

$$q_i = -\frac{u^3 \rho g}{12\mu} \Phi, i = -k\Phi, i \tag{3.3}$$

where the permeability of a single fracture is $u^2/12$, and the hydraulic conductivity is $K = \rho g u 3/12\mu$.

In Eq. (3.3), $u\ (x_i\ )$ is the actual radius of the fracture.

Variation of the fracture aperture occurs on a much smaller scale than the characteristic length of the model, and it is useful to obtain a relation between qi and Φ,i that is valid on the macroscale of the joint, but which neglects (when possible) the local variations of aperture. A first guess is to develop a relation of the same form as that of

Eq. (3.3), except that *uh* is now a macroparameter related to the Representative Elementary Area (REA) of the joint surface — i.e.,

$$q_i = -\frac{u^3 \rho g}{12\mu} \Phi, i \tag{3.4}$$

where *uh* (x_i) is the hydraulic aperture of the fracture

In this case it is assumed that *uh* = *um* which is not always the case. To this a modified cubic law is used in the code given by the following equation.

$$q_i = -\frac{u^3 \rho g}{12\mu F} \Phi, i \tag{3.5}$$

where *F* is a correction factor

Comparing equation (3.4) and (3.6), we obtain:

$$uh = fum = uh0 + f\Delta um$$

$$f = \frac{1}{F^{\frac{1}{3}}} \tag{3.6}$$

The joint conductivity, K, is defined (assuming one-dimensional flow)

$$k = -\frac{q}{\frac{d\Phi}{dx}} \tag{3.7}$$

Assuming the following dependence of the joint conductivity on hydraulic aperture:

$$k = -\frac{\rho g}{12\mu}(uh0 + f\Delta um^3) \tag{3.8}$$

we obtain

$$uh0 + f\Delta um = -(\frac{12\mu}{\rho g}\frac{q}{\frac{d\Phi}{dx}})^{\frac{1}{3}} \tag{3.9}$$

The unknown parameters $uh0$ and f can be calculated by linear regression of the experimental results.

The flow rate is a function of the fracture closure for two reasons:

1. The area (in cross-section) through which the fluid flows is reduced as the fracture closes; and

2. The area of actual contact between two fractures increases, making the flow more tortuous.

Although implementation of more complicated models is straightforward, the model implemented in *3DEC* uses the simplest approximation of joint behavior. Normal and shear joint stiffness are represented by linearly elastic springs.

The shear resistance of the joint is modeled by the Mohr- Coulomb condition with a prescribed dilation angle. It is assumed that *f* = 1.0, while *uh*0 and the residual hydraulic aperture *ures* are the model parameters.

3.3 Mohr Coulomb-slip joint models

This basic joint constitutive model is a generalization of the Coulomb friction law. This law works in a similar fashion both for contacts between rigid blocks and contacts between deformable blocks. Both shear and tensile failure are considered, and joint dilation is included.

In the elastic range, the behavior is governed by the joint normal and shear stiffness's, k_n andk_s .

The contact displacement increments are used to calculate the elastic force increments. The normal force increment, taking compressive force as positive, is

$$\Delta F^n = -k_n \Delta U^n A_c \tag{3.10}$$

and the shear force vector increment is

$$\Delta F_i^s = -k_n \Delta U_i^s A_c \tag{3.11}$$

where A_c= area of the contact.

The total normal force and shear force vectors are updated for the contact as

$$F^n = -F^n + \Delta F^n \tag{3.12}$$

and

$$F_i^s = -F_i^s + \Delta F_i^s \tag{3.13}$$

This instantaneous loss of strength approximates the "displacement-weakening" behavior of a fracture.

The new contact forces are corrected in the following manner (note that normal compressive force is positive):

For tensile failure if

$$F^n < \mathrm{T}_{\max},$$

then

$$F^n = \mathrm{T}_{\mathrm{residual}}$$

For shear failure if

$$\mathrm{F}^{\mathrm{s}} < F^s{}_{\max,}$$

then

$$\mathrm{F}^{s} < F^{s}{}_{i}\,\frac{F^{s}{}_{\max,}}{F^{s}} \tag{3.14}$$

where shear force magnitude F^{s} is given by

$$F^{s} = F^{s} = (F^{s}{}_{i} F^{s}{}_{i})^{\frac{1}{2}} \tag{3.15}$$

Dilation takes place only when the joint is slipping. The shear increment magnitude, ΔU^{s} is given by

$$\Delta U^{s} = (\Delta U^{s} \Delta U^{s})^{\frac{1}{2}} \tag{3.16}$$

This displacement leads to dilation of

$$\Delta U^{n}(dil) = \Delta U^{s} \tan\psi \tag{3.17}$$

where ψ is the dilation angle.

Dilation is a function of the direction of shearing. Dilation increases if the shear displacement increment is in the same direction as the total shear displacement, and it decreases if the shear increment is in the opposite direction.

For an intact joint (i.e., without previous slip or separation), the tensile normal force is limited to

$$T_{max} = -T\ A_c \tag{3.18}$$

where T is the joint tensile strength

The maximum shear force allowed is given by

$$F^s{}_{max} = cA_c + F^n \tan\phi \tag{3.19}$$

where c and ϕ are the joint cohesion [stress] and friction angle.

When the failure is identified at the contact (in either tension or shear), and residual values are specified, the tensile strength and cohesion are set to the residual values:

$$T_{max} = T_{residual}$$

$$F^s_{max} = C_{residual}A_c + F^n tan\,\emptyset \tag{3.20}$$

CHAPTER 4

MODELING AND SIMULATION IN 3DEC

4.1 Model construction

The geomechanical model is an important aspect when studying a tight gas sand reservoir and contributes to the accuracy of the results. The geomechanical model incorporates various properties such as elastic moduli, rock strength, and pore pressure, as well as the magnitude and orientations of principal stresses. The domain for the geomechanical model was built and imported into Itasca's 3DEC. The model was constructed using 3DEC version 4.10.100.The values used for geomechanical properties were typical values for a depth of 3,300 meters as obtained from the literature (Osorio, 2009). All of the values are tabulated in Table 4-1.

The discrete fracture network was created for the RPSEA (Research Partnership to Secure Energy for America) project. This model was taken and then tailored to avoid the computational expense. To do this some educated guesses were made and the size of model was reduced. This helps in making the model more compatible with the UFES simulator and also to make the simulations run in a practically feasible time. Even if the number of fractures were reduced the discarded fractures were only those with poor connectivity. The model shown in Figure 4-1 had more than 70,000 fractures.

Table 4-1 Values used for the model, depth of 3396 meters

Dimensions		200X 200 X 20	feet
Fluid Density		1000	kg/m3
Fluid viscosity		1	cp
Bulk Density		2500	kg/m3
Bulk Modulus K		9.20E+09	Pa
Shear Modulus G		5.52E+09	Pa
Fracture normal Stiffness		1.7e6	Pa
Fracture Shear Stiffness		1.7e6	Pa
Fracture initial Aperture		.5e-4	m
Far Field Stress (vertical)	σ_1	5.10E+07	Pa
Far Field Stress (Horizontal)	σ_2	4.49E+07	Pa
	σ_3	6.90E+07	Pa
Initial Reservoir Pore Pressure		3.10E+07	Pa

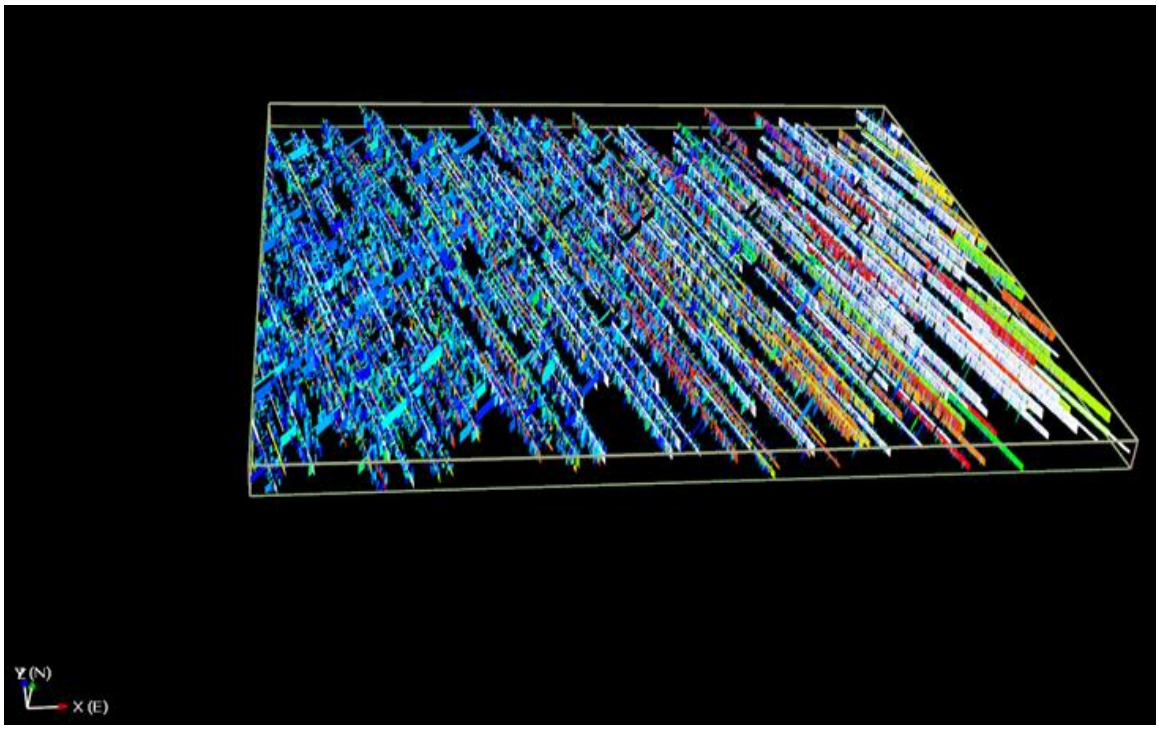

Figure 4- 1 The discrete fracture network from Golder and Associates

Some fractures were connected to fracture network while some fractures were isolated from the fracture network. These isolated fractures were discarded, while reducing the fracture network domain. Running a simulation for this great number of fractures is extremely difficult and time consuming and might take several years. To avoid this computational expense an educated guess was made in reducing the number of fractures as mentioned. Thus fractures of "high importance" were considered and isolated fractures were discarded. This modified fracture network was then created geometrically and meshed in the software CUBIT developed by Sandia National Laboratories.

The prototype Discrete Fracture Network (DFN) model that was created had approximately 100 vertical fractures. The discrete fracture network set consists of two different sets of fractures. The first set of fractures is long and spread across the domain. The longer fractures strike at N103E. Shorter fractures strike at N123E. All of the

fractures do not essentially intersect. The fractures were imposed over a domain of 2200 X 2200 X 20 meters. The conditions in the reservoir resemble the environment at a depth of 3300 meters. Figure 4-2 shows this modified fracture network. This fracture network geometry was then imported into ITASCA's 3DEC distinct element code.

4.2 Modeling in commercial software 3DEC

Boundary Conditions and Rock Characteristics: - The rock was modeled as a very low permeability medium with a density of 2,500 kg/m^3, a shear modulus of 9.20 GPa, bulk modulus of 5.52 GPa and a Poisons ratio of 0.25. For a depth of 3300 meters maximum principal stress, intermediate principal stress, minimum principal stress were taken as 69 MPa, 51 MPa, and 44.9 MPa, respectively. These properties for the rock

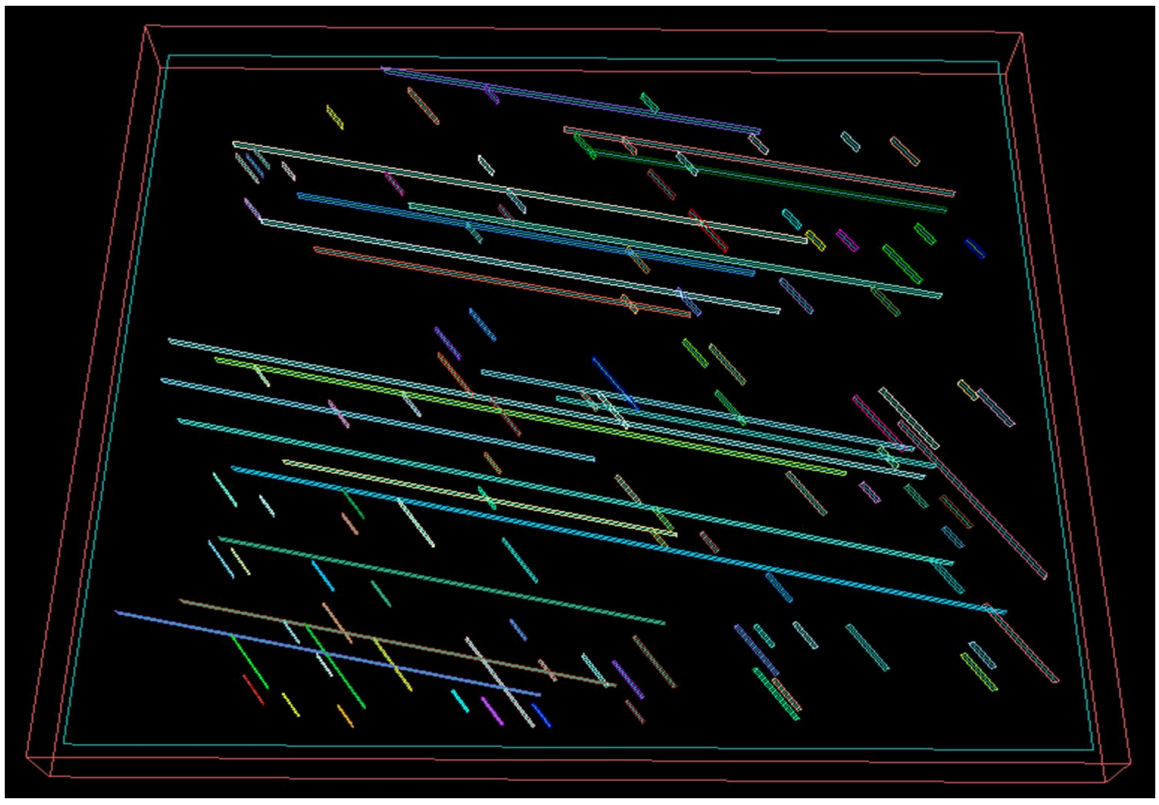

Figure 4- 2 Fracture network created in CUBIT software

matrix and in-situ stress field were obtained from the literature data for tight rock formations (Osorio, 2009).

4.2.1 Fracture parameters

The fracture parameters used in the simulation had an initial stiffness value of 1.7 MPa, and an initial aperture of 0.5 mm. The simulations were run with a Mohr-Coulomb Slip model. The fracture normal stiffness controls the normal closure/opening resulting from changes in the normal effective stress. The Mohr-Coulomb model also reproduces dilation/contraction induced during fracture shearing. The fracture shear strength depends on the friction angle, the effective normal stress acting on the fracture and the cohesion. The fracture cohesion value used in the model was 1 MPa.

4-2.2 Calculation sequence in 3DEC

The steps in 3DEC are as follows:

Mechanical equilibrium is achieved by neglecting the fluid flow in the fracture and taking into account the in-situ stress field.

Coupling the hydro-mechanical calculations to achieve flow equilibrium.

With equilibrium reached simulating calculation of fluid and geomechanics.

The model shown in Figure 4-2 was imported into ITASCA's 3DEC and the simulations were carried out. The fluid was injected along the hydraulic fractures and is shown by the arrow in the Figure 4-3. The variations in the pore pressure and stresses were recorded. The results for the pore pressures can be seen in Figure 4-3.

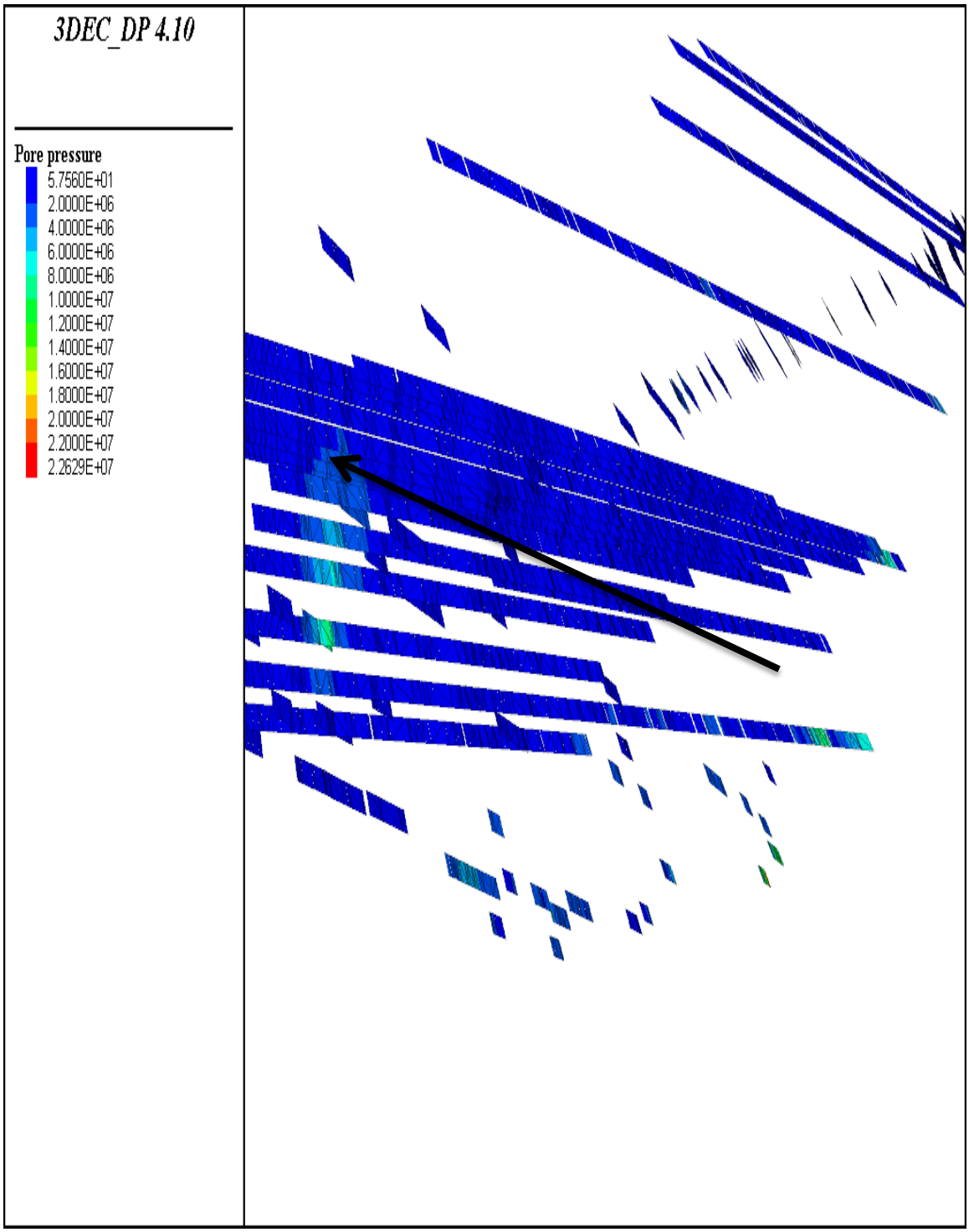

Figure 4- 3 Pore pressure in the fracture network after injection shown with the arrow pointing toward injection point source

The simulated results were not as expected and hence a further step was taken to ensure the proper fracture connectivity. The fracture network generated by cubit was modified to check the fracture descriptions resulting in better connectivity. Also the number of fractures was reduced by removing the nonconnecting isolated fractures. This helped to improve the fracture connectivity. This resulted in geometry with 40 well connected fractures as shown in Figure 4-4. The model with recreated fracture network was then meshed.

Figure 4-5 shows the pore pressure distribution after injection for approximately 2 seconds at the rate of $0.1325 m^3$/sec. As expected the highest value of pore pressure was recorded at the point of injection. As the point of observation moved farther away from point of injection the pore pressure decreased and at distances far away from point of injection pore pressure remained unchanged from the initial value.

Figure 4-6 is a similar representation showing apertures after a very brief injection period (approximately 2 seconds). (The fluid has entered fractures not necessarily preferentially oriented to the principal stresses).

Figure 4-5 and Figure 4-6 show the flow of the fluid (water) in the fracture network. The fluid follows a path which is governed by the in-situ shear stresses. The injected fluid causes the apertures to grow and thus shows how the fluid is flowing in the fracture network. The extensive and dense fracture needs extremely large simulation time.

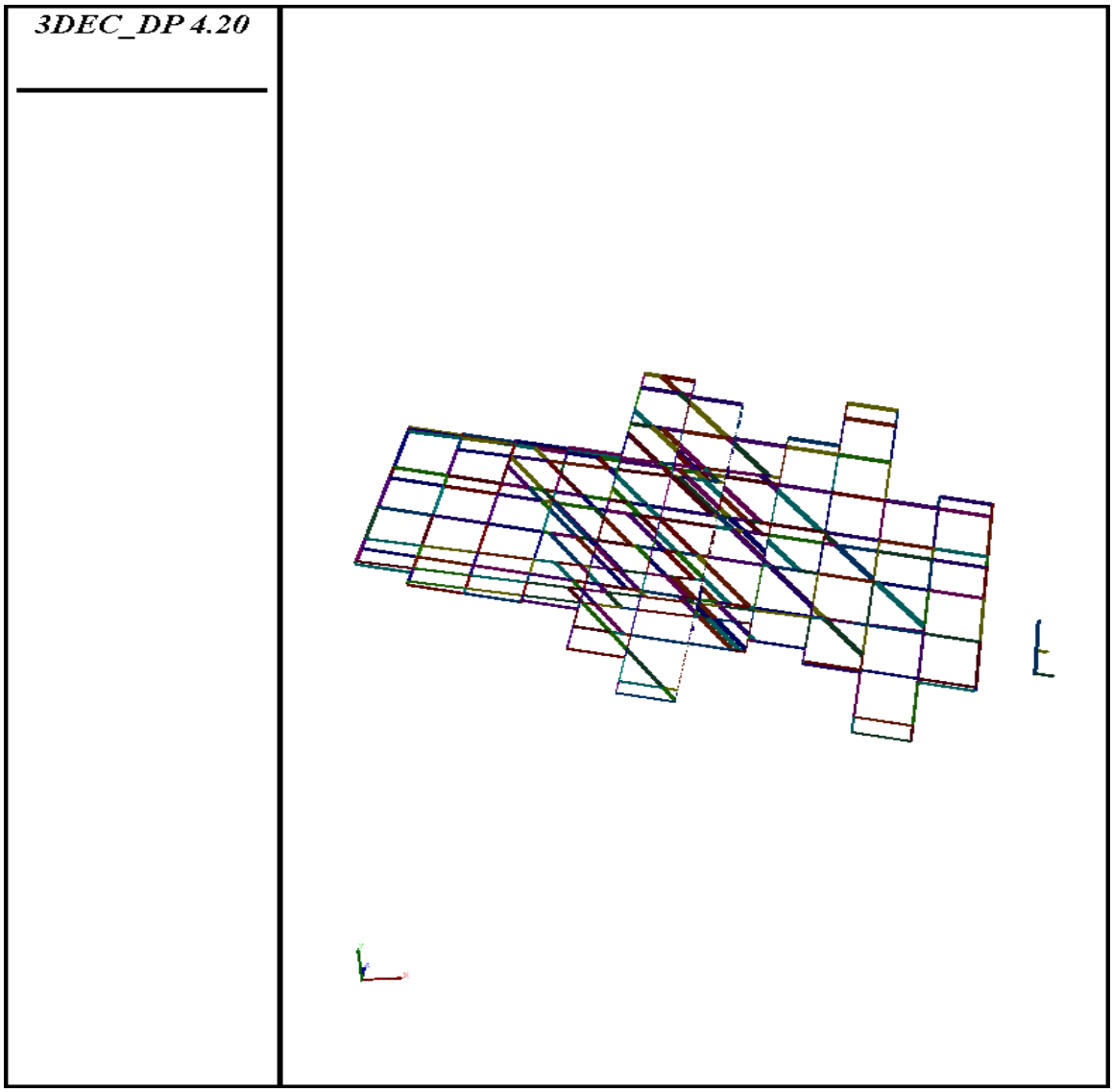

Figure 4- 4 Fracture network created for distinct element code where the fluid flow is possible.

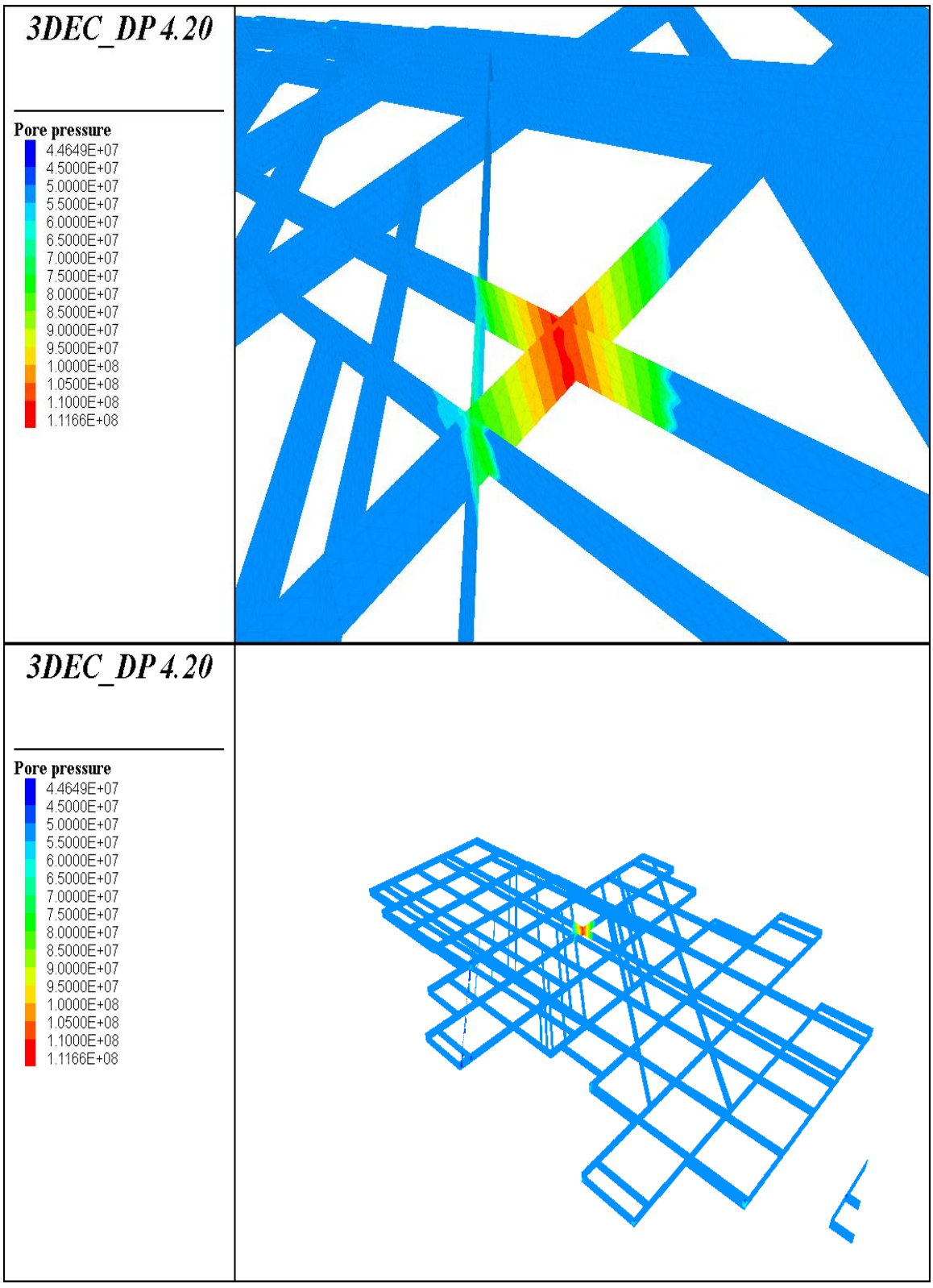

Figure 4-5 Pore pressure distribution profile in fracture network after hydraulic stimulation

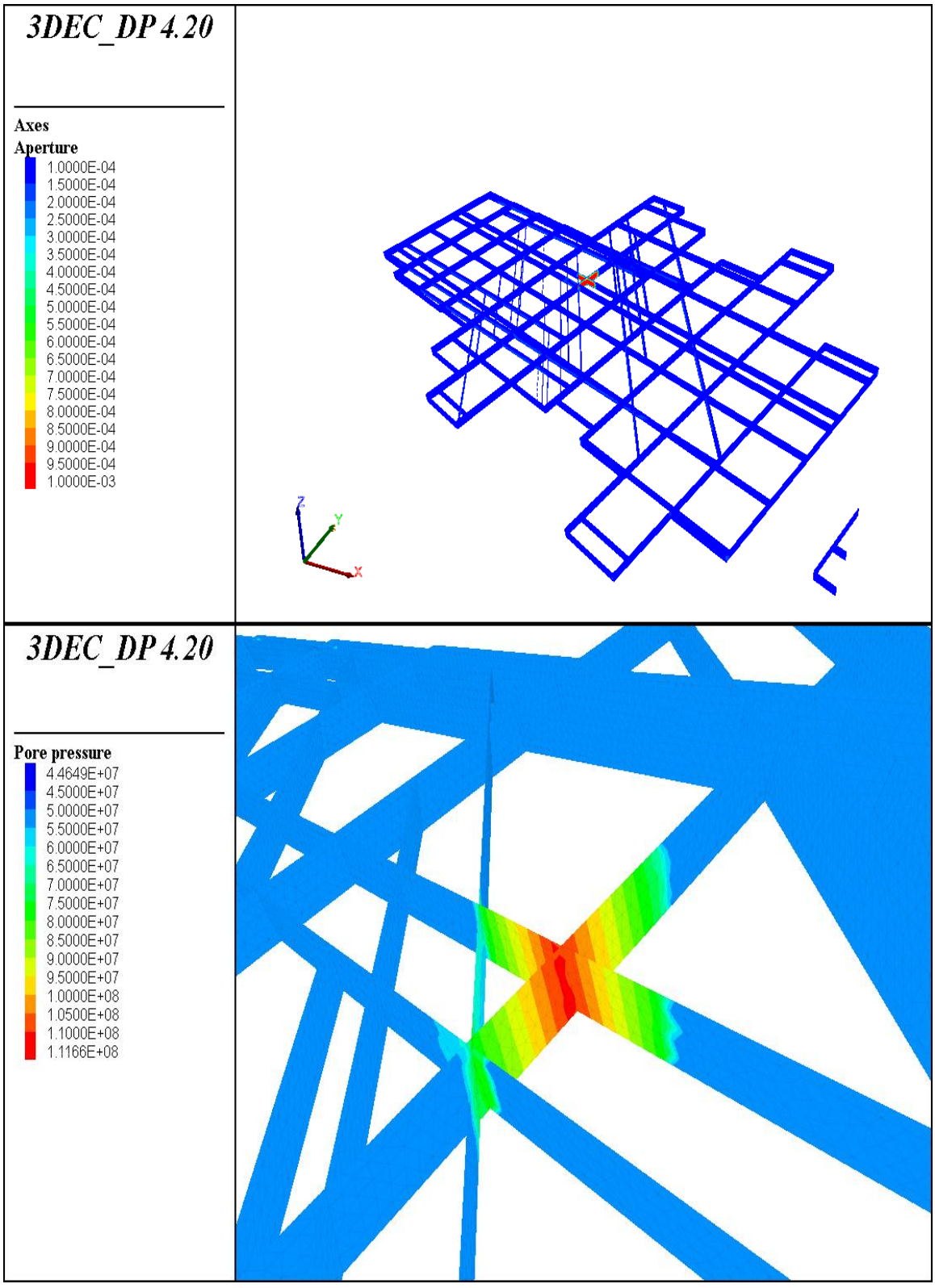

Figure 4-6 Aperture growths seen in stimulated fracture network model due to hydraulic stimulation

4.3 Parametric sensitivity study

A domain with size of 200 x 200 x 20 was created with 4 discrete fractures intersected by a single fracture at an angle of 45° (except when model size was varied). The simulations were performed for the in-situ conditions described in Table 4-1. The parameters considered were injection rate, fracture spacing, and fracture orientation. The in-situ stresses are shown in the accompanying figures.

4.3.1 Effect of Injection Rate

One of the stimuli to changes in pore pressure in the model is variation in fluid volume which is altered by injection at a fixed volumetric rate. This becomes more important with no flow boundary conditions applied in the model. Hence, the flow and geomechanical calculations were carried out in this model at the injection rates of 0.16 m^3/min (Fig 4.7) and 0.32 m^3/min. The fluid was injected as a point source in the fracture with longest length and is shown by arrow in Figure 4-7.

Figures 4-7 and 4-8 shows pore pressure distribution at the end of the injection period along with discharge rates. As seen from these two figures higher injection rate resulted in higher pore pressure at individual nodes. The highest value of pore pressure was recorded at the point of injection. The pore pressure at the point away from the injection point was lower as compared to the pore pressure at the injection point. The pore pressure values in lower injection rate are much lower in comparison to pore pressure values observed with higher injection rates.

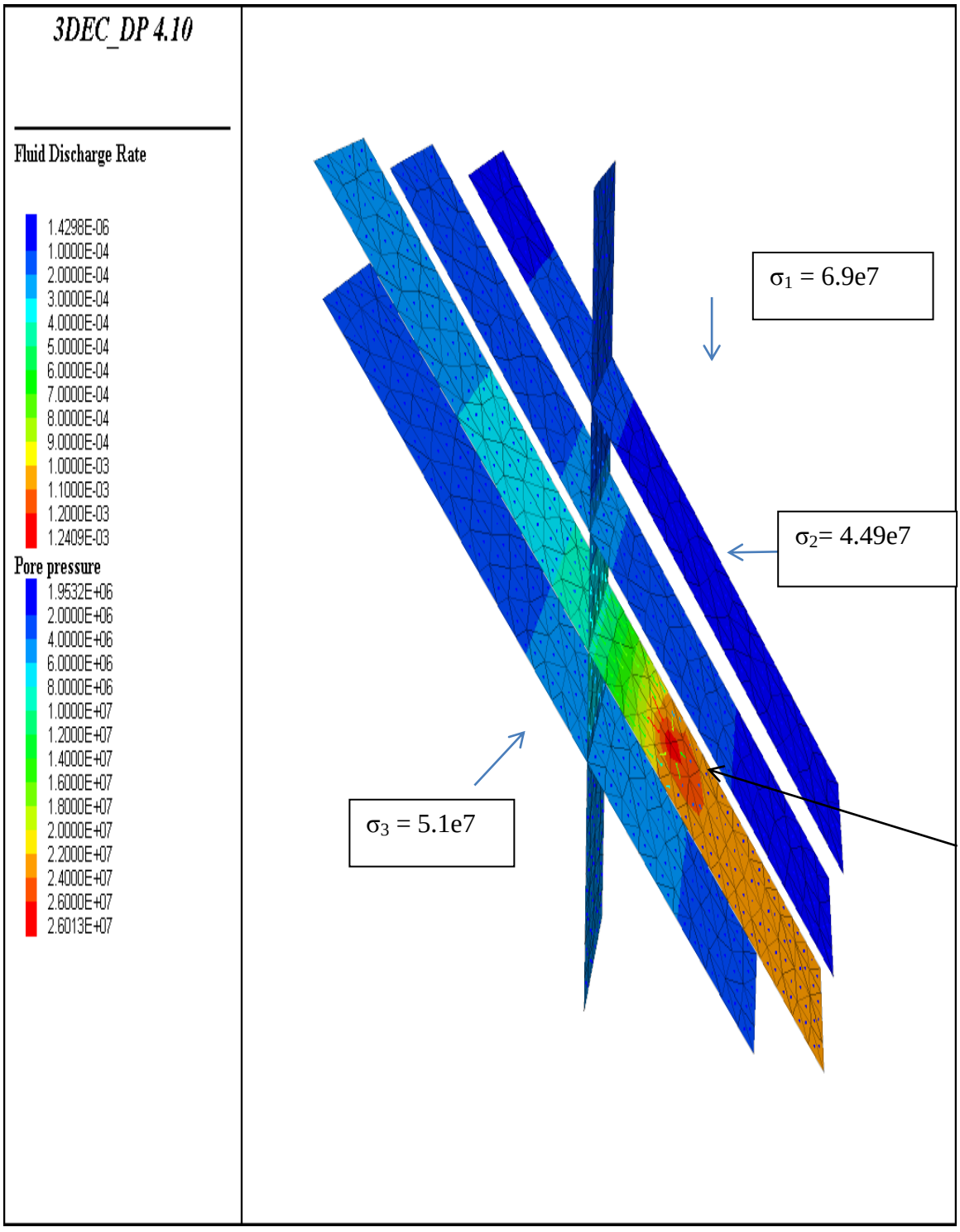

Figure 4- 7 Measured fluid discharge rate and the variation in the pore pressure for the model having 4 inclined fractures with one vertical fracture when the discharge rate was 0.16 m^3/min

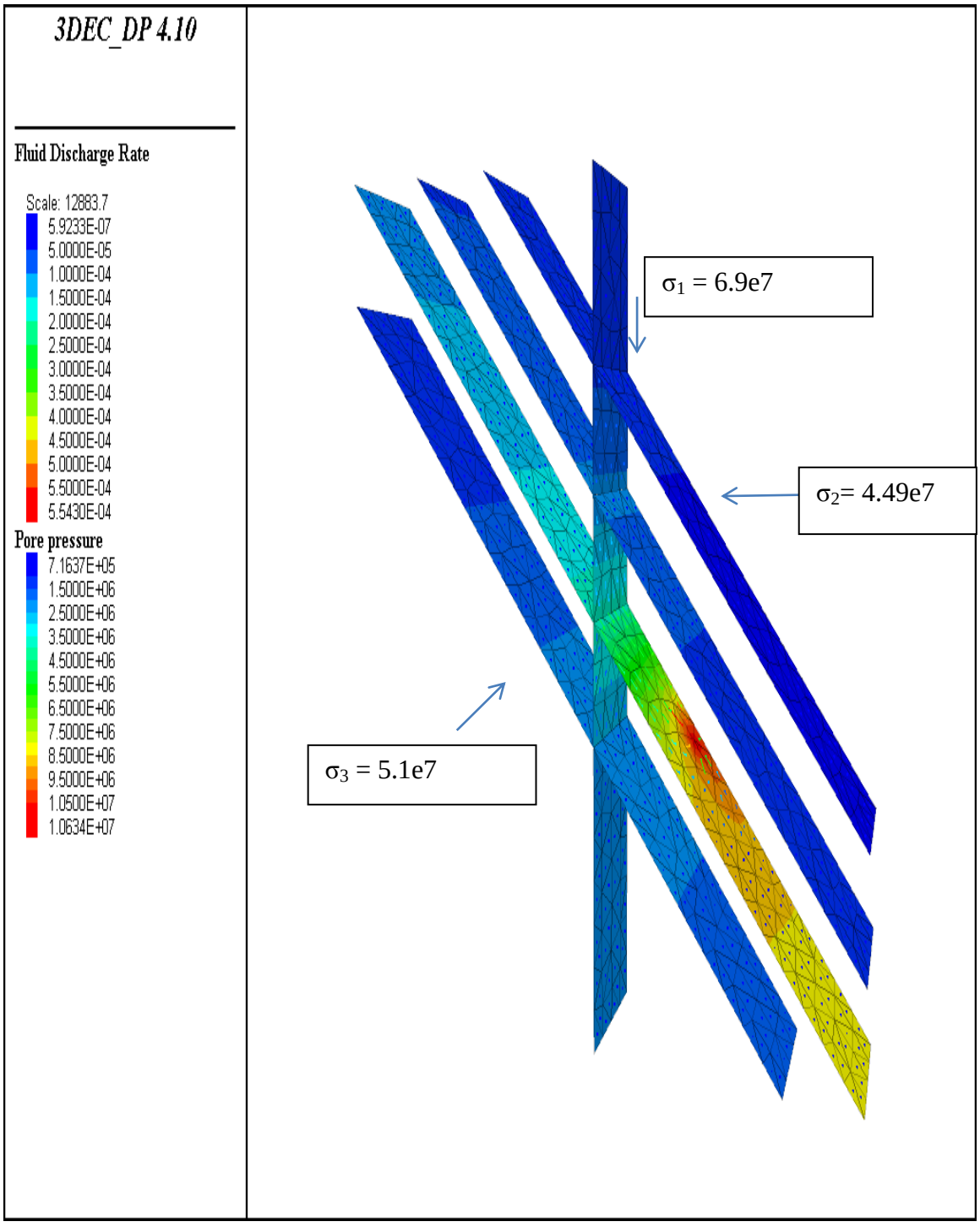

Figure 4- 8 Measured fluid discharge rate and the variation in the pore pressure for the model having 4 inclined fractures with one vertical fracture when the discharge rate was 0.32 m^3/min

An examination of the normal displacement vector field showed that an increase in the injection rate results in an increase in hydraulic fracture aperture by ~40%-50% at the point of injection. In Figure 4-9 for example, the joint normal displacements appear to spread far field in comparison to the lower rate simulation shown in Figure 4-10. For tight gas reservoirs this large increase in fracture conductivity which makes the recovery swifter also justifies the cost of higher hydraulic power.

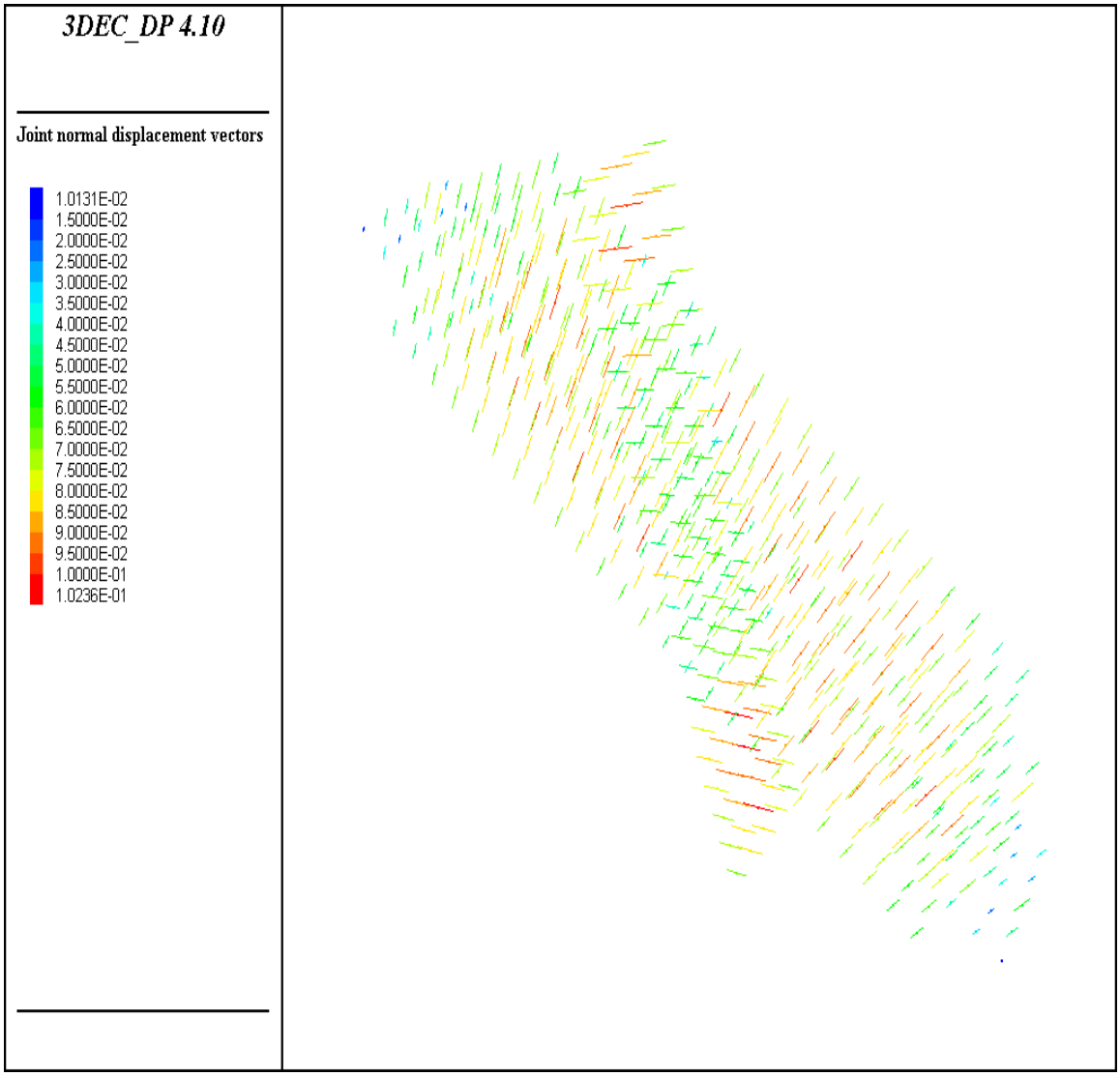

Figure 4- 9 The displacement vector profiles shown for the model with injection rate of $0.32m^3/min$

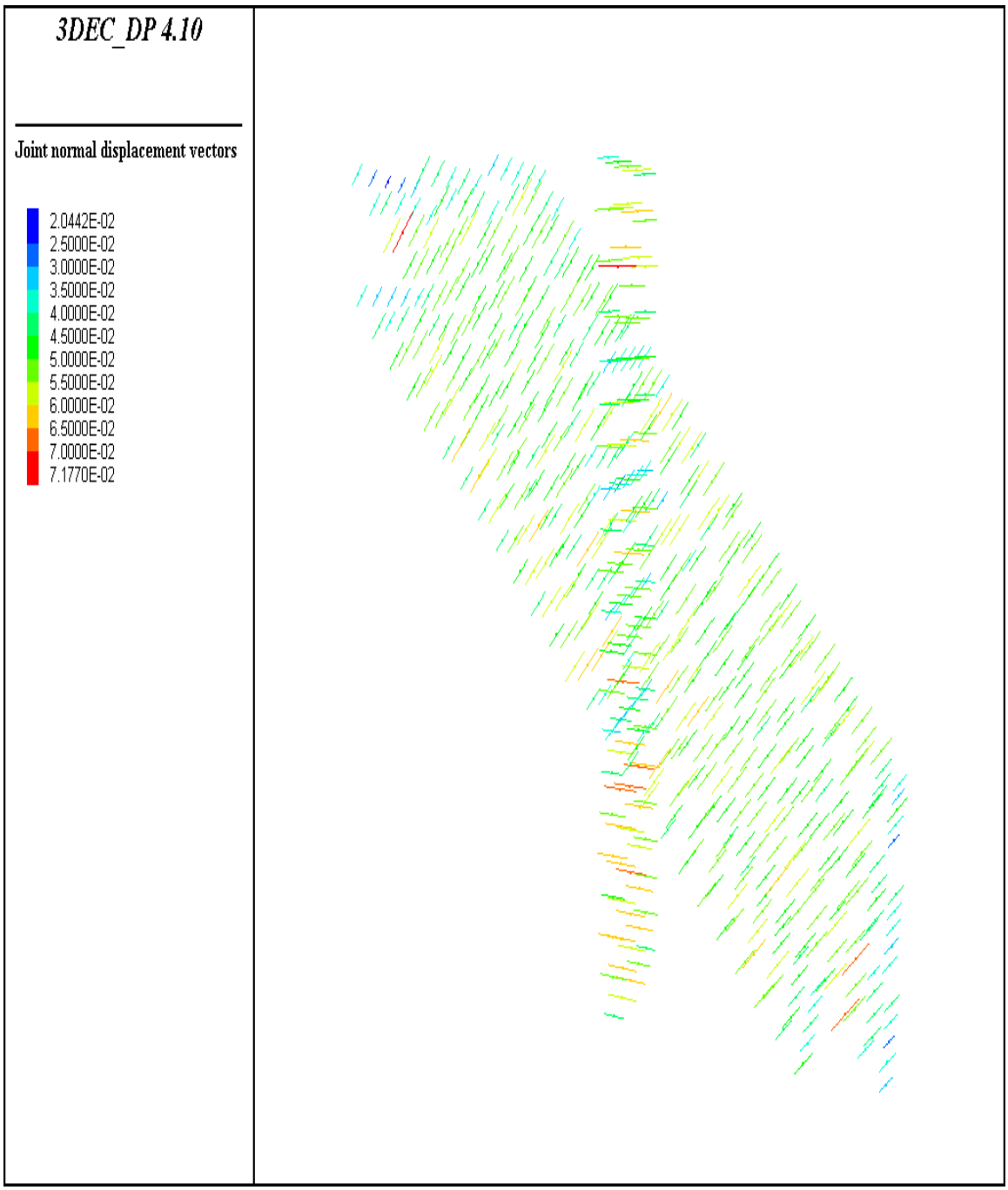

Figure 4- 10 The displacement vector profiles shown for the model with injection rate of 0.16m3/min

4.3.2 Effect of Fracture Spacing

Fracture spacing determines the time fluid takes to enter individual fractures. This ultimately results in higher fluid buildups in the fractures with smaller spacing. Hence two simulations were performed with distances of 20m and 5m between fractures. Pore pressures and discharge rates for these two cases are shown in Figures 4-11 and 4-12, respectively. When the fracture spacing was 5m, the system reached higher pore pressures (Figure 4-12) in comparison to when the fracture spacing was 20m (Figure 4-11). This is attributed to shorter flow paths into the inclined fractures with smaller spacing ensuring higher discharge and larger pressure rise.

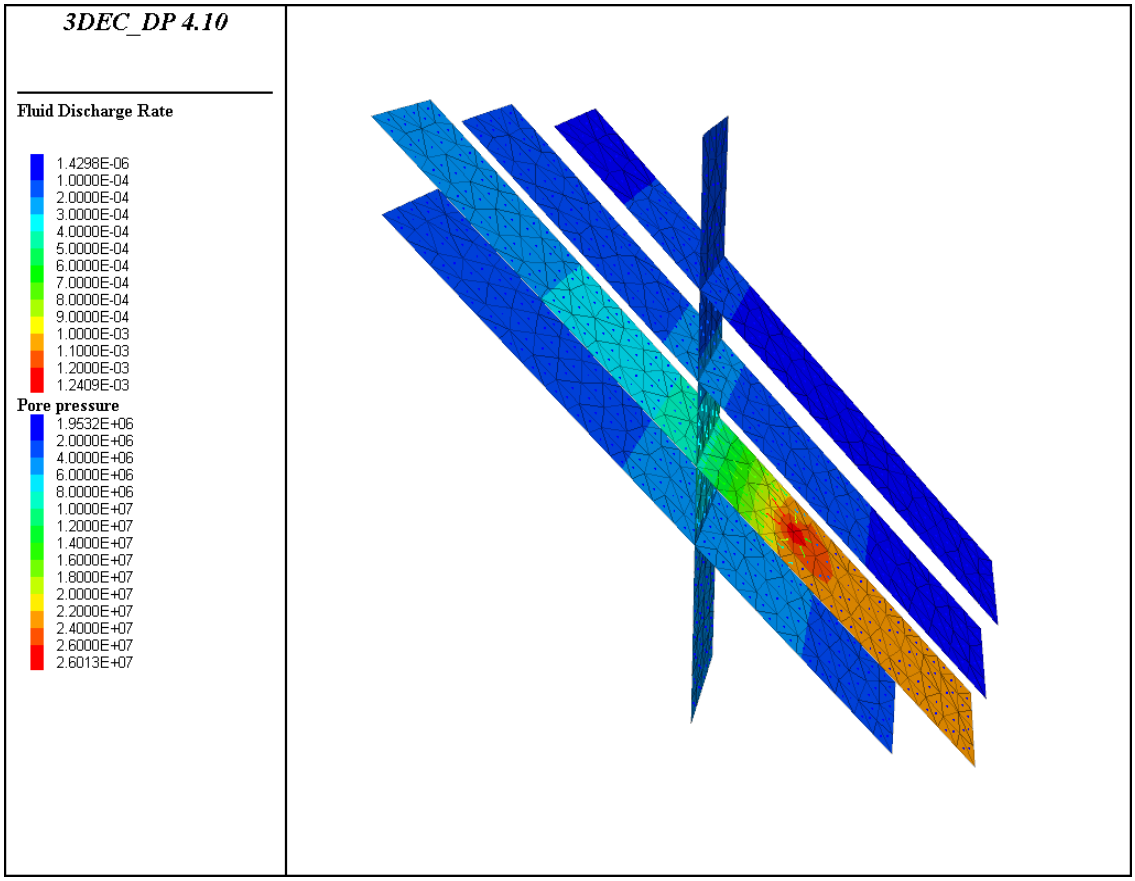

Figure 4- 11 The pore pressure distribution profile with fluid discharge rate vectors for model having fracture spacing of 20 m

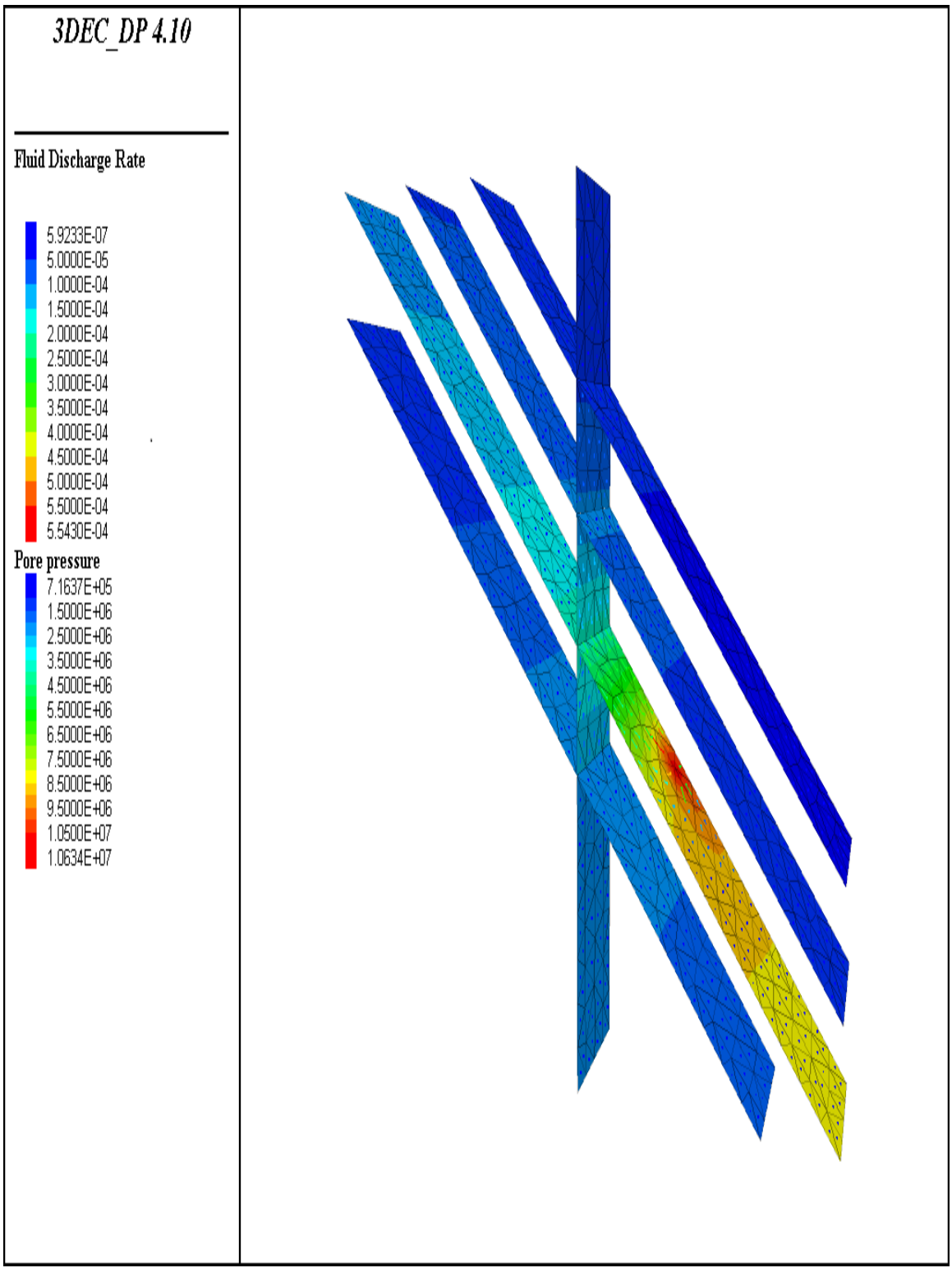

Figure 4- 12 The pore pressure distribution profile with fluid discharge rate vectors for model having fracture spacing of 5 m

4.3.3 Dip Angle and Dip Direction

The orientation of fracture with respect to in-situ stress field determines the effective stresses acting on fractures. The higher the effective stress on fractures the higher is the resistances to the fluid flow and hence two orientations were simulated. The fracture parameters, rock characteristics, and boundary conditions were all unchanged.

In the first case the dip direction 90º and dip angle of 0º the effective normal stress on the fractures was more (Figure 4-13) than that observed in the second case with dip direction of 90º and dip angle of 45º (Figure 4-14). This reduction in effective normal stress gave rise to higher pore pressure in the fractures.

In the third case the dip direction 0º and dip angle of 0º the effective normal stress on the four fractures (Figures 4-15) were more as compared to fourth case which had dip direction of 45º and dip angle of 0º (Figure 4-16). This reduction in effective normal stress gave rise to higher pore pressure in the fractures having dip direction of 45º.

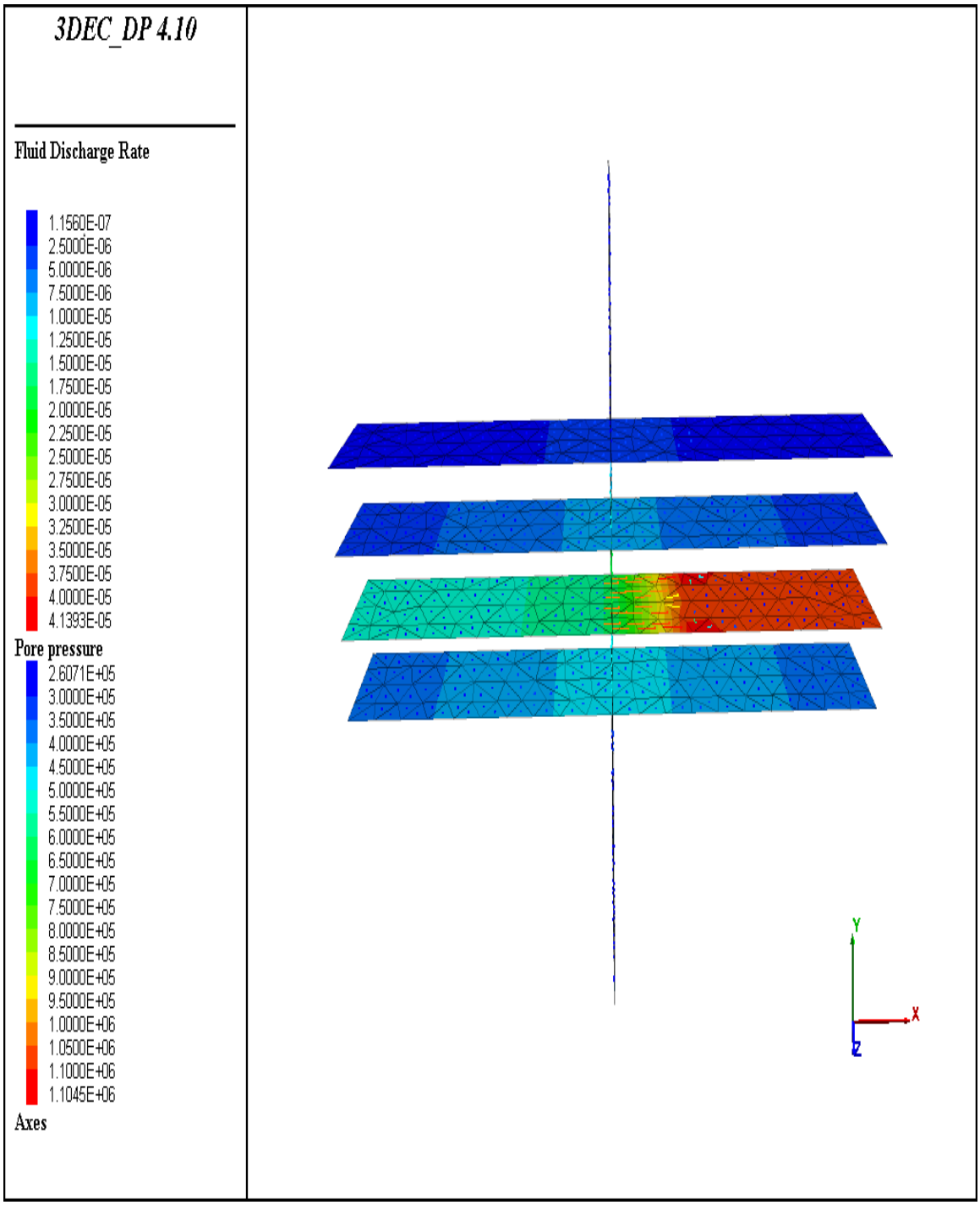

Figure 4- 13 Measured fluid discharge rate and the variation in the pore pressure for the model with 4 horizontal fractures

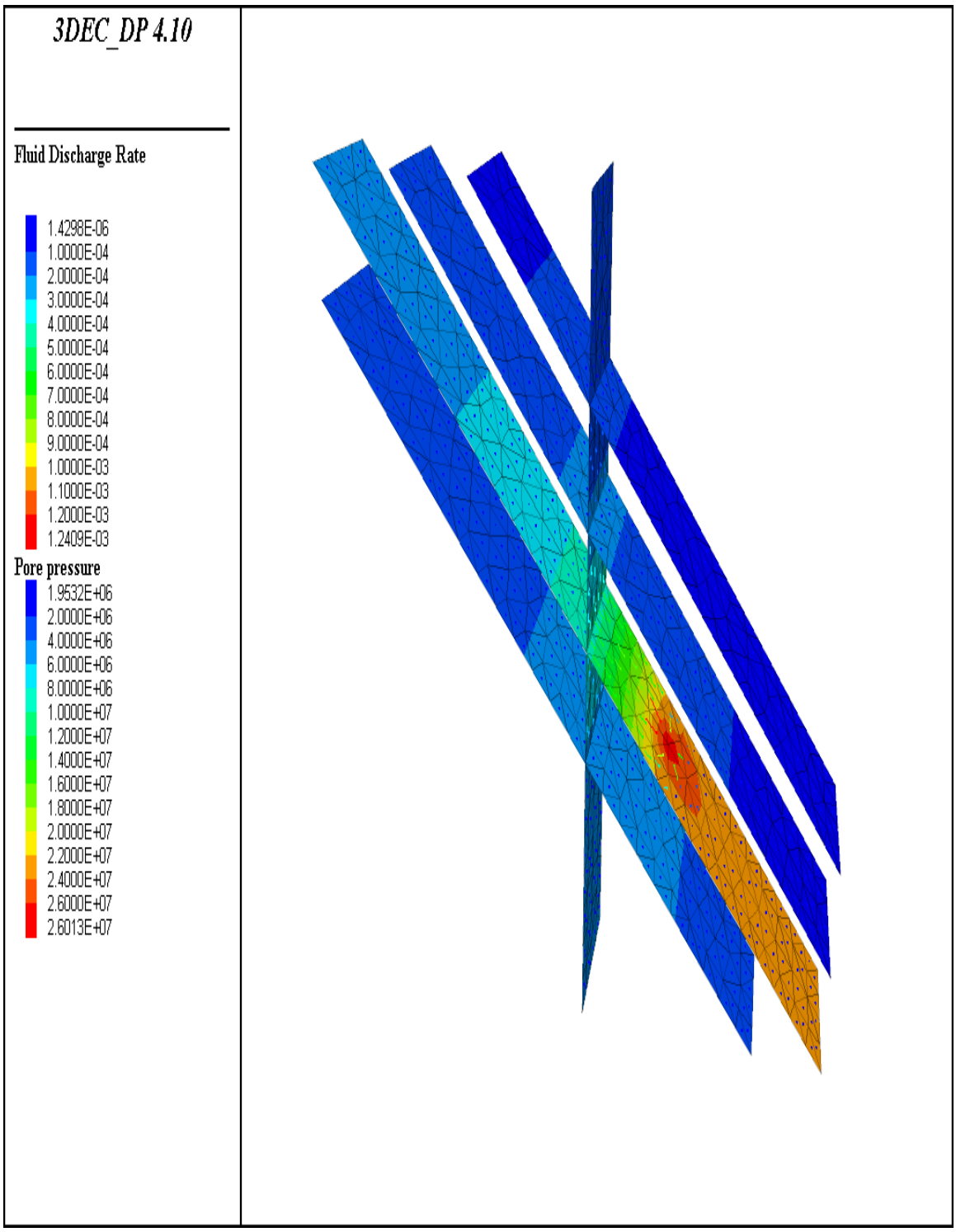

Figure 4- 14 Measured fluid discharge rate and the variation in the pore pressure for the model with 4 horizontal fractures inclined at 45º

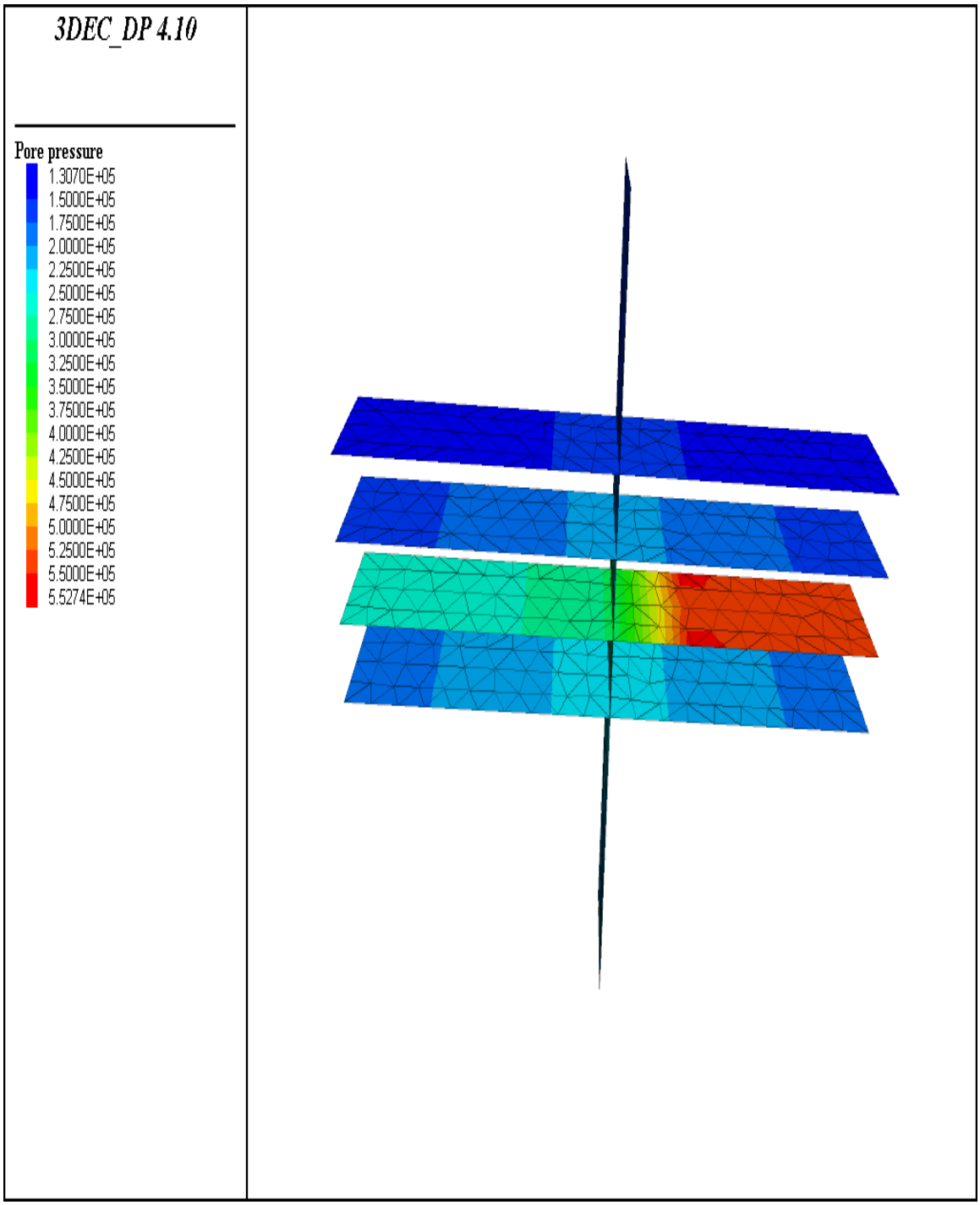

Figure 4- 15 Measured fluid discharge rate and the variation in the pore pressure for the model with 4 horizontal fractures rate with dip of 90º and dd of 0

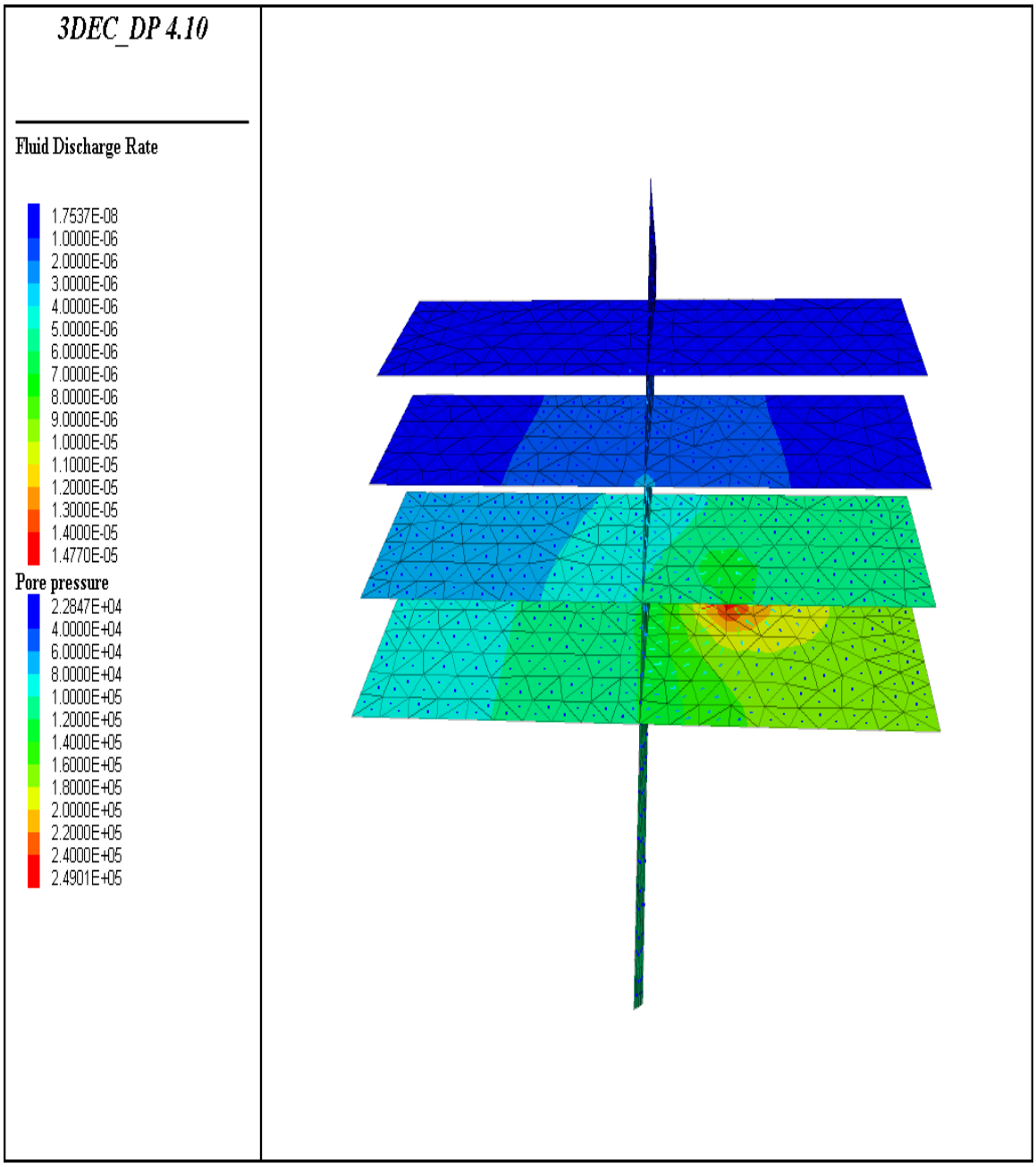

Figure 4- 16 Measured fluid discharge rate and the variation in the pore pressure for the model with 4 horizontal fractures rate with dip of 90º and dd of 45

CHAPTER 5

SIMULATIONS IN TIGHT GAS RESERVOIR USING UFES

The UFES simulator was used for running the initial tight gas simulation by doing some necessary changes in the Simulator code. The simulations were carried out in the continuous volume finite element method (CVFEM) module of the simulator. The details are explained in the following section.

Modifications were made in black oil module of continuous volume finite element simulator (CVFEMBO2) of UFES simulator for the tight gas simulation.

The basic differential form of Darcy's Law for horizontal laminar flow is valid for describing the flow of both gas and liquid systems. For radial gas flow, the Darcy equation of the form was chosen.

$$q_g = \frac{0.001127}{\mu_g} kA * \frac{\partial P}{\partial z} \qquad 5.1$$

$$q_{gr} = \frac{0.001127(2\Pi rh)k}{\mu_g} k * \frac{\partial P}{\partial r} \qquad 5.2$$

where

q_{gr} is gas flow rate at radius r,

r is radial distance, ft

h is zone thickness, ft

μ_g is gas viscosity in centipoises

p is pressure in psi

0.001127 is a conversion constant to field units.

The gas flow rate is expressed in Mscf/day.

5.1 Simulations in UFES

5.1.1 Modeling

Reservoir geometry was created with dimensions of 2200 X 2200 X 200 meters. The geometry included the two distinct fracture sets, one with 67 shorter fractures and the other with 25 longer fractures. This geometry was created in the meshing tool CUBIT. This meshed geometry was then processed and then exported in the UFES simulator. To evaluate the effect of hydraulic fracture on gas recovery, two models were created, one with the hydraulic fracture and another model without hydraulic fracture. The matrix permeability and fracture permeability was varied. This set of simulations also demonstrated the role of permeability of fracture and the matrix. The simulation runs carried out for this study are tabulated in Table 5.1

First, simulation was carried out to see the effect of hydraulic fracturing on the flow. The simulation results were extracted for regular time intervals.

Case 1: In this numerical runs, the fracture sets had low permeability of 100 millidarcies and 10 millidarcies for short and long fractures, respectively. The matrix

Table 5.1 Simulation matrix

No	[1]	2	3	4	5	6
No of Days	20	100	200	360	360	360
BHP at well (Psi)	2700	2700	2700	2700	2700	2700
Fracture permeability (mD) (Long fractures)	100,0,100	100,0,100	100,0,100	100,0,100	100,0,100	1000,0,1000
Fracture permeability (mD) Short fracture	10,0,10	10,0,10	10,0,10	10,0,10	10,0,10	100,0,100

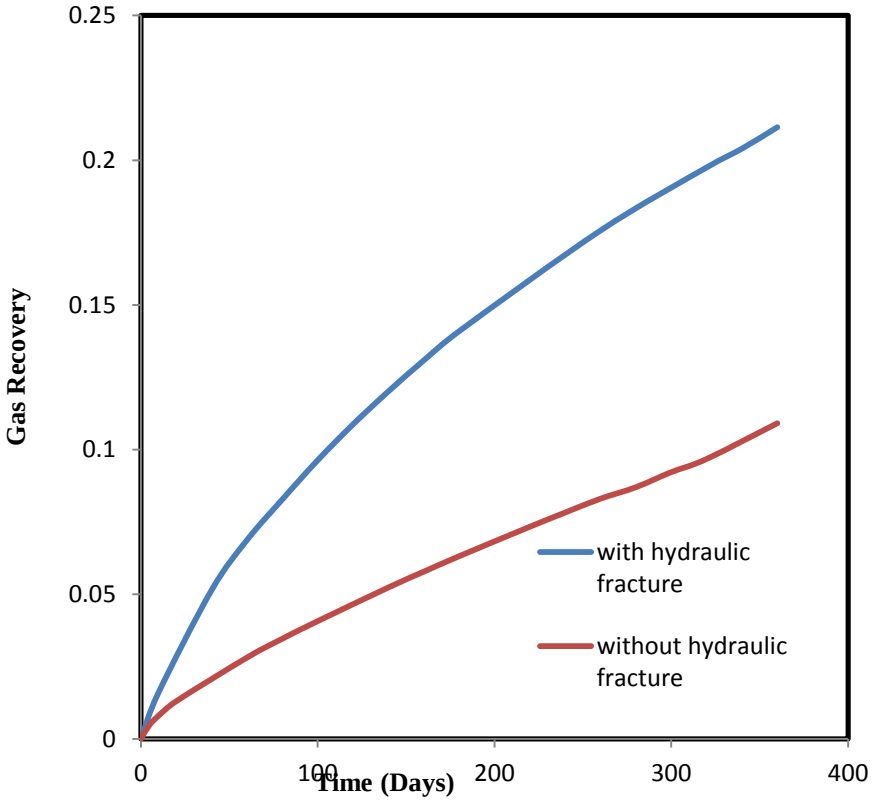

Figure 5- 1 Gas recovery vs. time

permeability was kept very low at 0.05 millidarcies. Figure 5-1 shows the gas recovery curves obtained with and without presence of hydraulic fracture.

As seen from Figure 5-1 the gas recovery was enhanced with the presence of hydraulic fracture by approximately 50% for a recovery time of 360 days. This can be attributed to increase in permeability of the fracture network because of the hydraulic fracture. This was evident from the snapshots of the pore pressure distribution shown in Figures 5-2 to 5-7. In Figures 5-2 and 5-3 the gas pressure at the location shown by arrow indicates the lowering of gas pressure because of presence of hydraulic fracture. Thus, presence of hydraulic fracture greatly improves the gas recovery from low permeability formations.

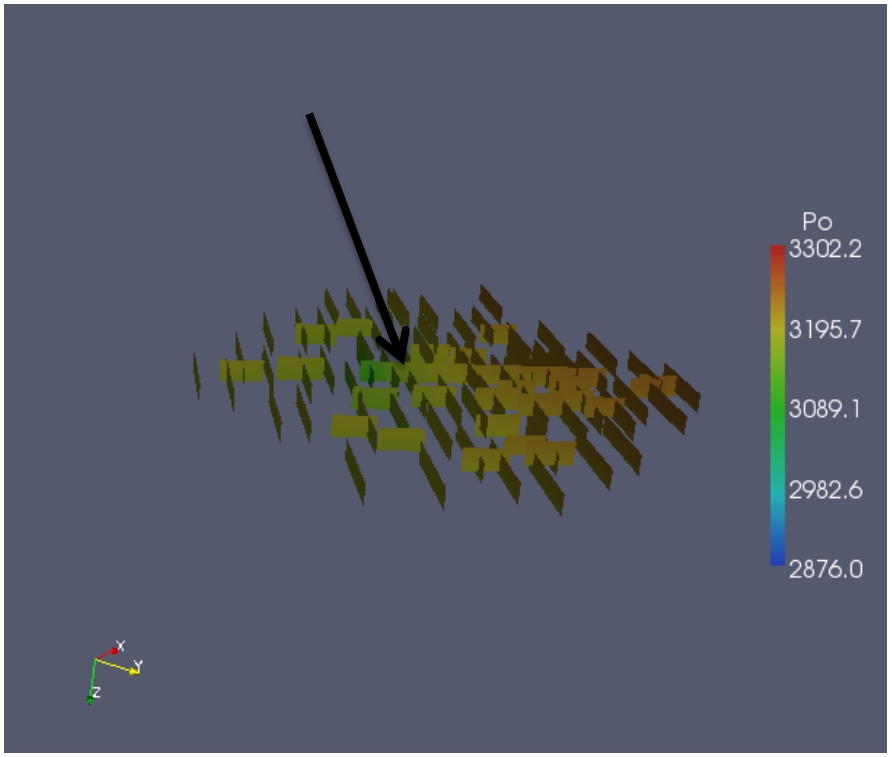

Figure 5- 2 Gas pressure in fracture network without hydraulic fracture after 20 days of injection

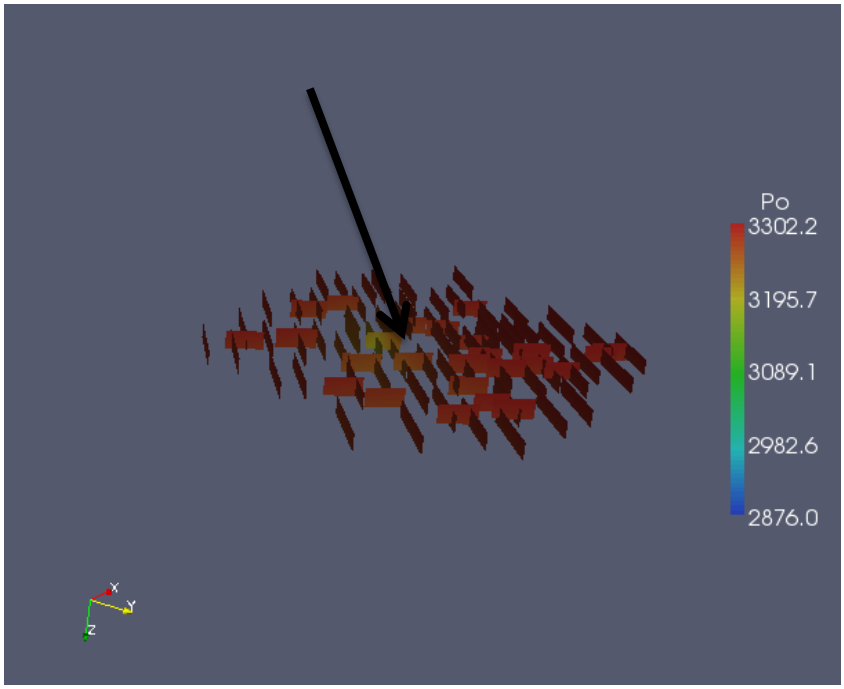

Figure 5- 3 Gas pressure in fracture network with hydraulic fracture after 20 days of injection

Figure 5-4 shows the decline in gas pressure without the presence of hydraulic fracture after 360 days of injection and Figure 5-5 shows the decline in gas pressure with hydraulic fracture after 360 days of injection. Figure 5-6 shows the decline in gas pressure in the matrix with the presence of hydraulic fracture after 360 days of injection and Figure 5-7 shows the decline in gas pressure in the matrix without hydraulic fracture after 360 days of injection.

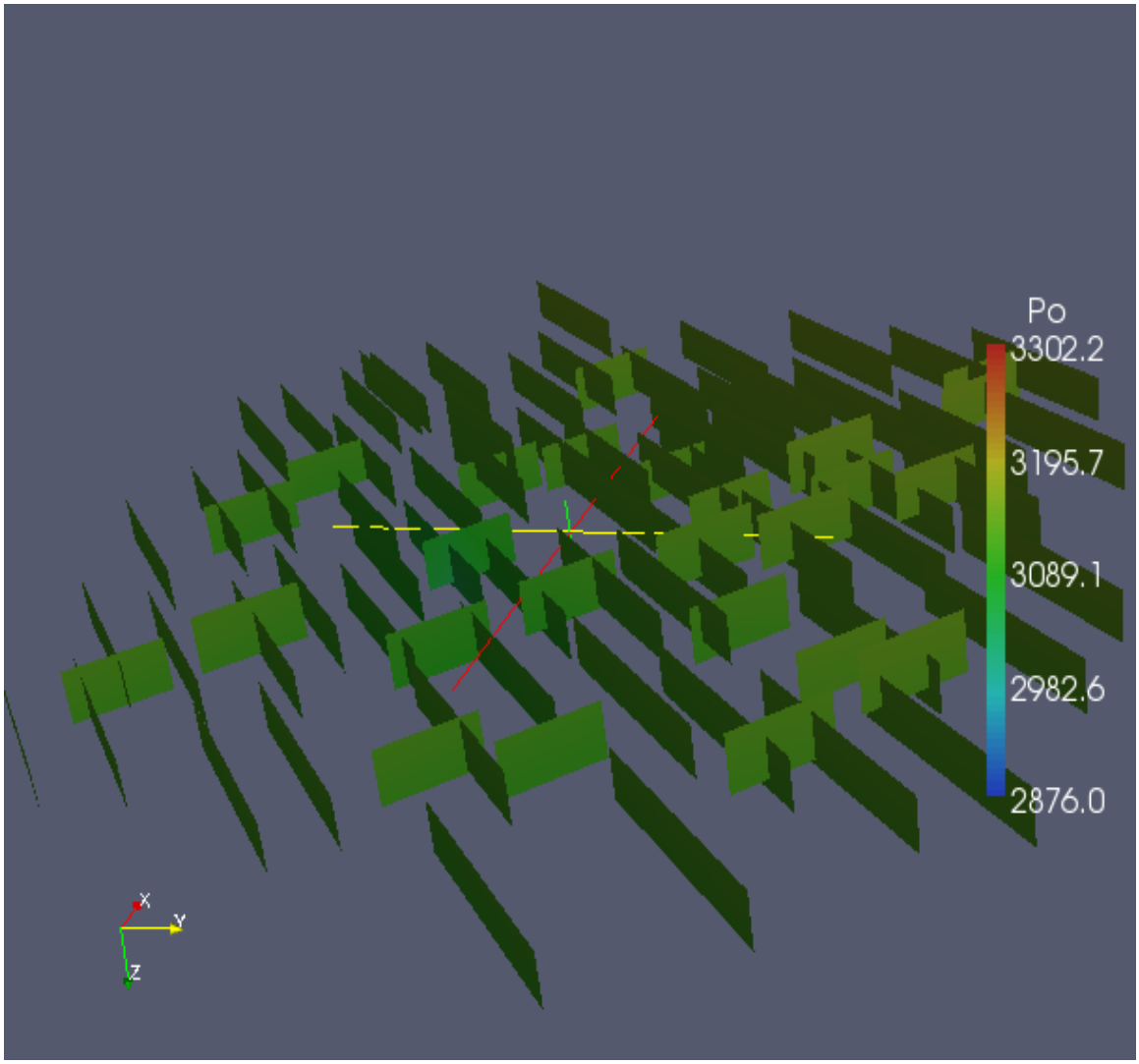

Figure 5- 4 Gas pressure in fracture network with hydraulic fracture after 360 days of injection

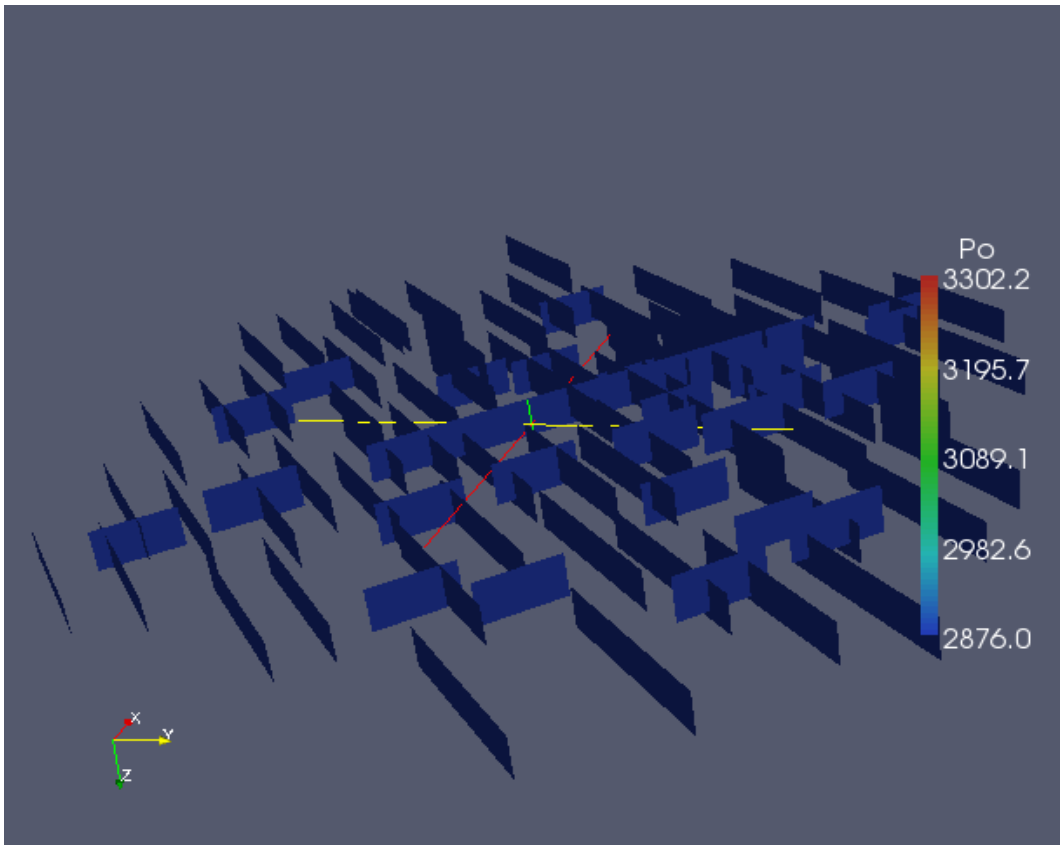

Figure 5- 5 Gas pressure in fracture network with hydraulic fracture after 360 days

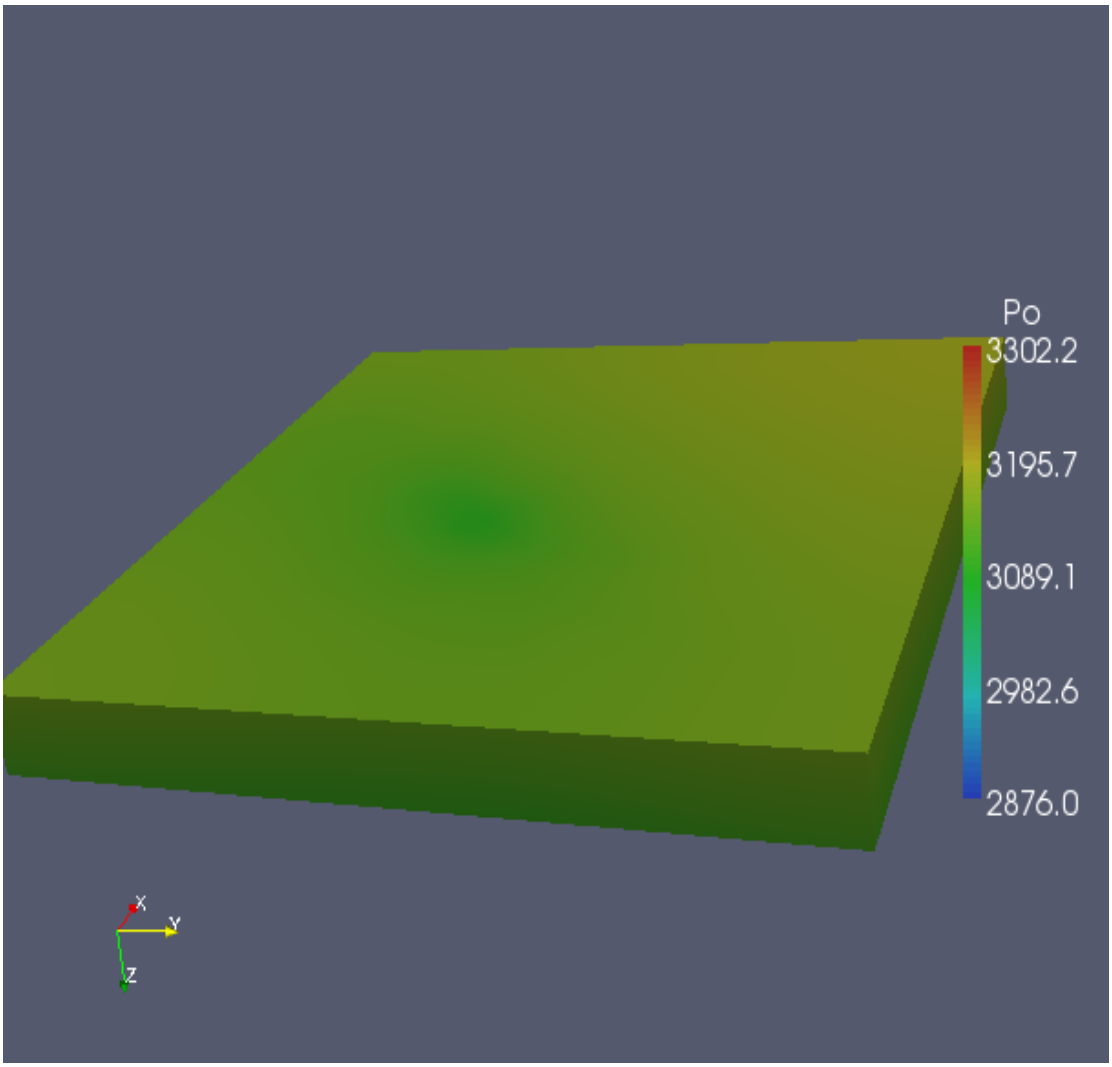

Figure 5- 6 Gas pressure in matrix without hydraulic fracture after 360 days

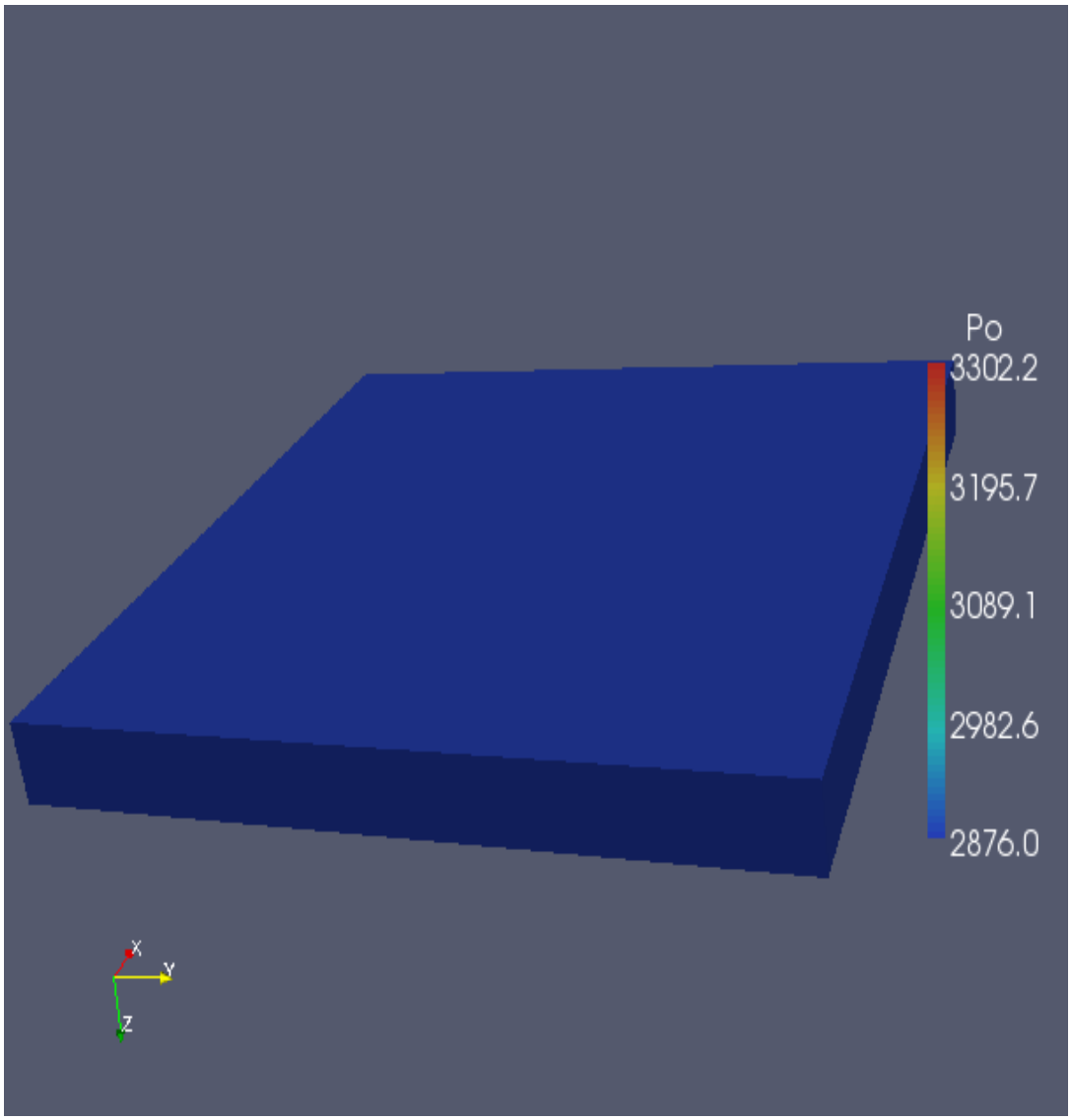

Figure 5- 7 Gas pressure in matrix with hydraulic fracture after 360 days

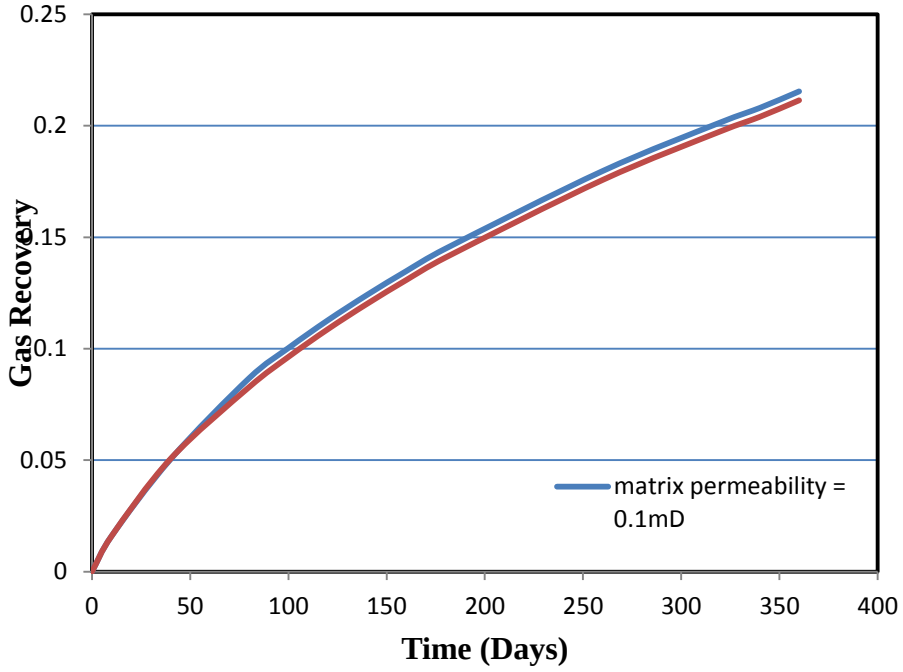

Figure 5- 8 Gas recovery plots with different matrix permeabilities.

Case 2: In this numerical run, the fracture sets had permeability of 100 millidarcies and 10 millidarcies for short and long fractures, respectively. Two values of matrix permeability that evaluated were 0.05 millidarcies to 0.1millidarcies. Figure 5-8 shows the gas recovery curves obtained for these numerical exercises.

As seen from Figure 5-8 there was no significant increase in gas recovery numbers. This was expected since the volume of the gas in the fracture is orders of magnitude smaller than the volume of gas present in the matrix. Hence any increase in the matrix permeability did not significantly improve the gas recovery.

Case 3: In these numerical runs, two set of permeability values were used for the fracture sets with ratio of permeability of longer fractures to that of shorter fractures being kept constant. In one set the permeability for longer fracture was 100 millidarcies and the shorter fracture was 1000 millidarcies. In the second set the permeability for long

fractures was 10 and for short fracture was 100 millidarcies. The matrix permeability was 0.1 millidarcies. Figure 5-3 shows the gas recovery curves for these runs.

As seen from Figure 5-9 significantly higher gas recovery was obtained with higher fracture permeabilities. Higher permeabilities in fracture enabled lower resistance to fluid path allowing more gas to be produced. This is advocated by the snapshot in Figures 5-10 to 5-13. These figures show the gas pressure distribution in the fracture network and rock matrix. High permeability fractures showed lower gas pressures as a result of improved gas flow, and gas pressure distribution in the matrix also evidently showed lower values compared to those in rock matrix with low permeability fractures.

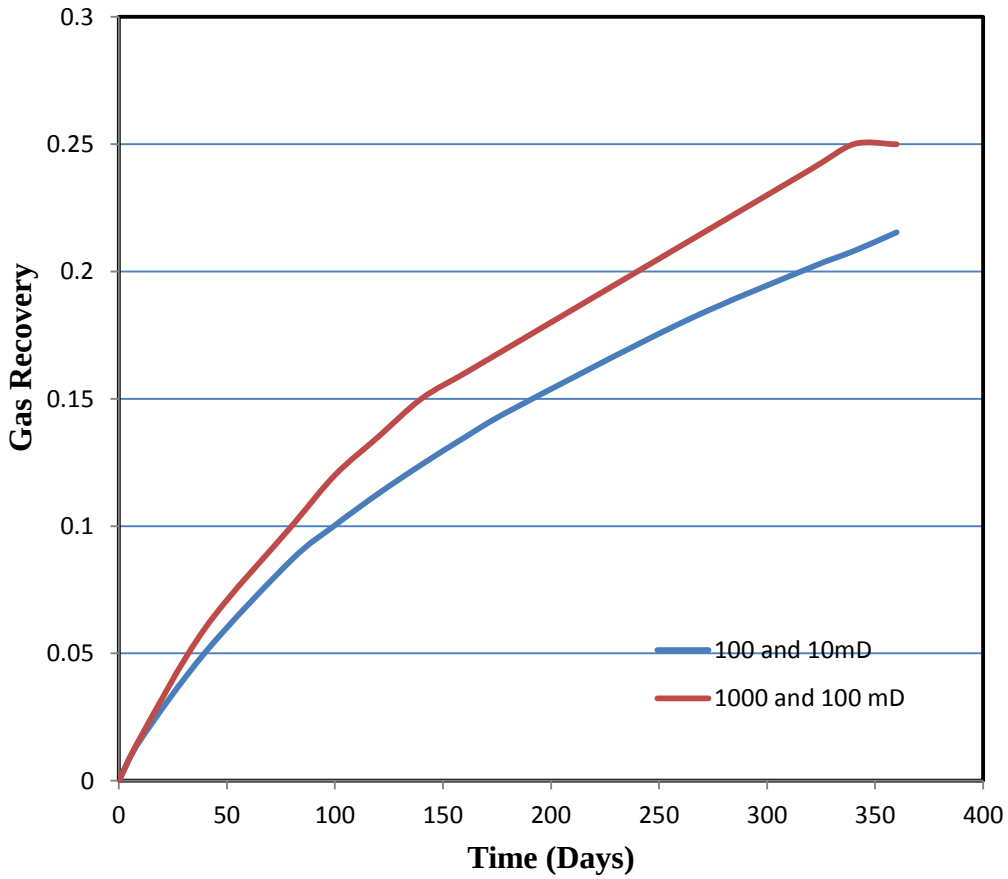

Figure 5- 9 Plot of gas recovery vs. time for different fracture permeabilities

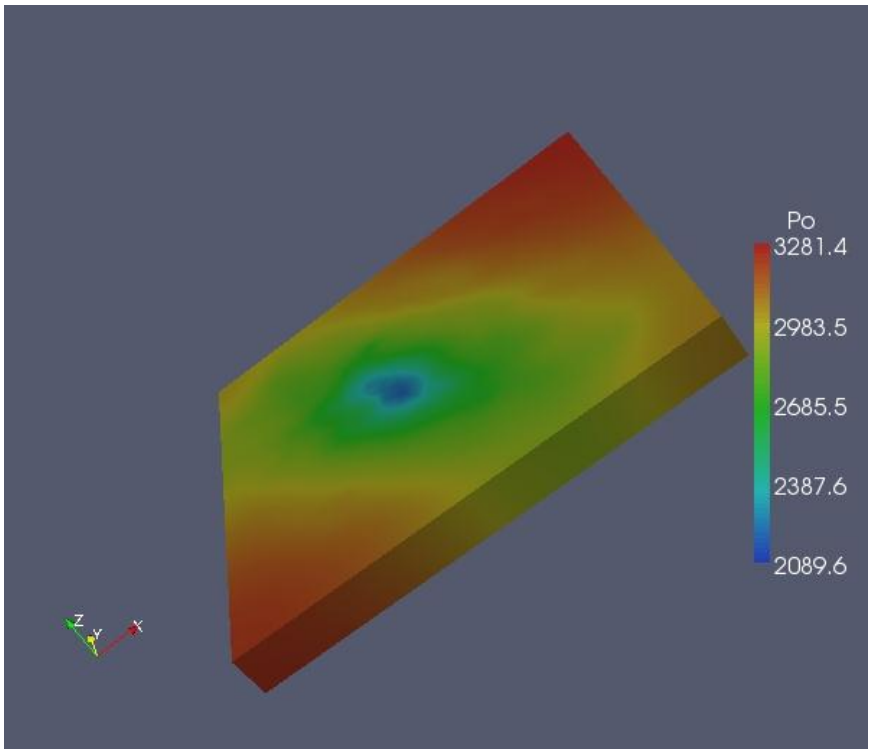

Figure 5- 10 Gas network in matrix without hydraulic fracture

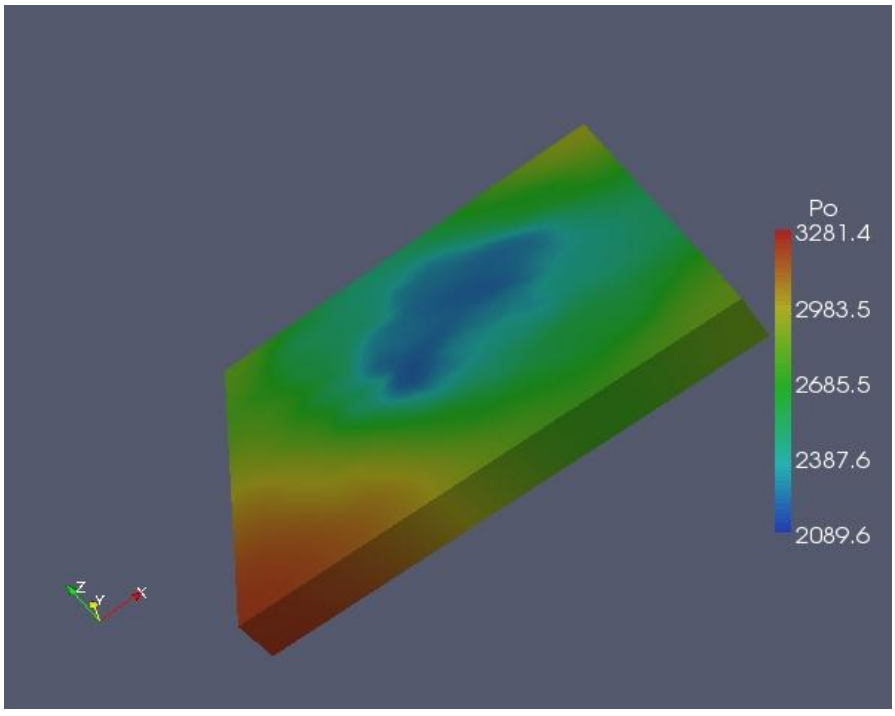

Figure 5- 11 Gas recovery in matrix network without hydraulic fracture

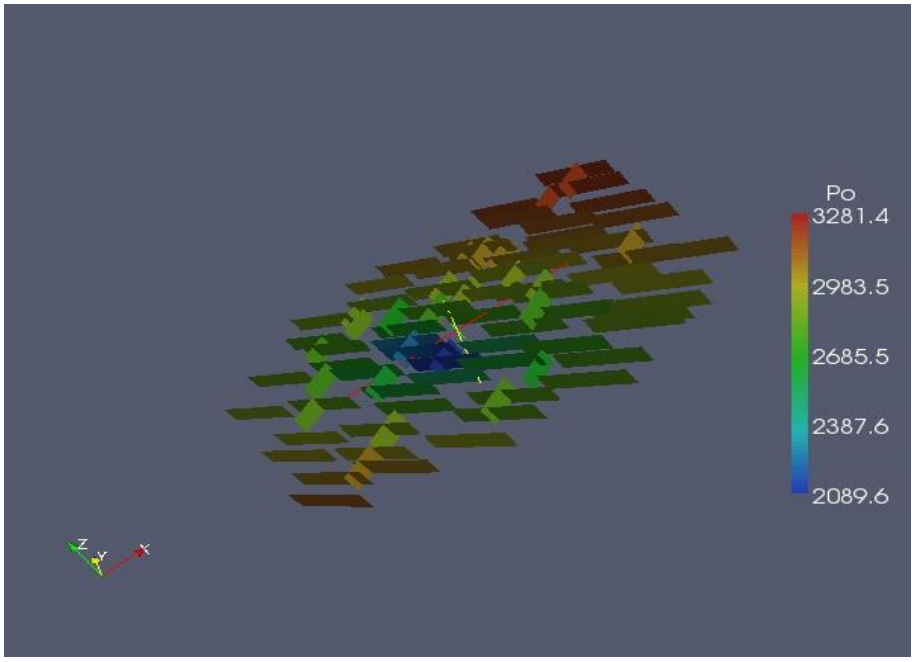

Figure 5- 12 Gas recovery in fracture network without hydraulic fracture

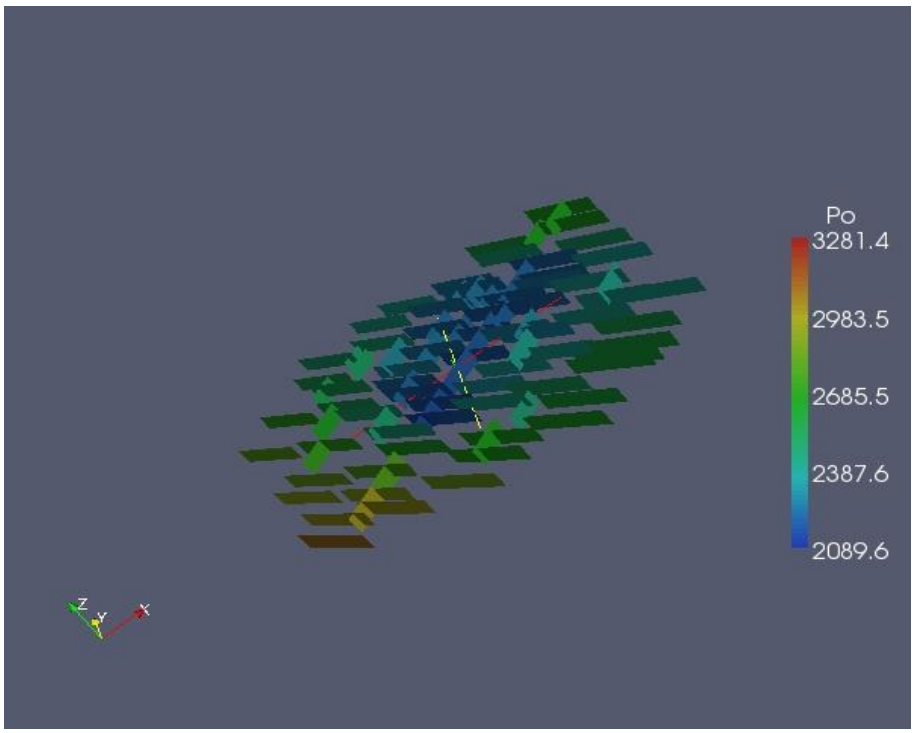

Figure 5- 13 Gas recovery in fracture network with hydraulic fracture

As evident from results discussed above introduction of hydraulic fracture improves gas recovery significantly. However gas recovery also depends on other factor like permeability of existing fractures, rock permeability and other factor which may be beyond the scope of this study.

This study was primarily focused on fluid flow aspects of tight gas formations. Hydraulic fracturing definitely increases the gas recovery. There is marked improvement in the recovery by making these fractures even more permeable. An approximately 20 % more gas was recovered when the permeability was increased by factor of 10. Tight gas formations in the source rock are inherently less permeable and hence a modest by factor of 2 in matrix permeability did not significantly affect the product recovery. A summary of all three cases has been represented in Figure 5-14 shown below. As seen from figure hydraulic fracturing along with high permeability definitely opens new opportunity for product recovery in tight gas formations. However, a note of caution should be included here with the fact that gas recovery may change over the long run of more than 5 years.

Figure 5-14 shows that the case with higher fracture permeability had better recovery of gas compared to the cases with low fracture permeability. There were no significant increases in recovery with increasing matrix permeability**.**

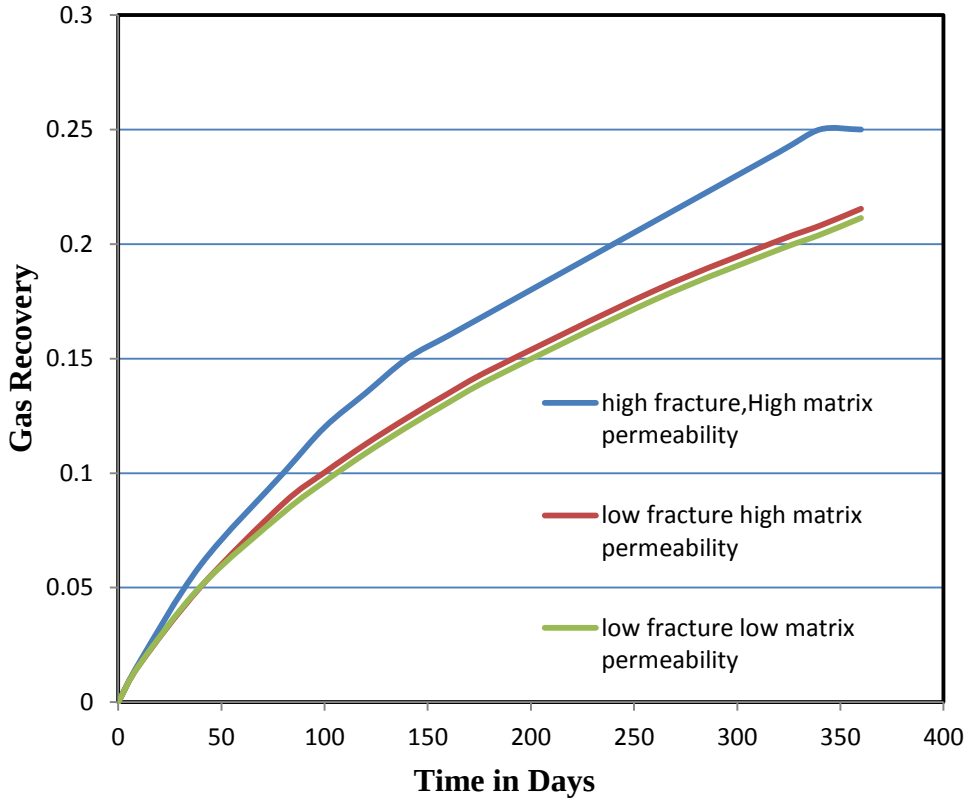

Figure 5- 14 Comparision of amount of gas recoverd against time in all three cases

CHAPTER 6

CONCLUSION

A detailed simulation study of the fracture network based on fracture orientation, fracture spacing, injection rate, and model size assist in locating where the fluid should be injected and how to recover gas more economically. Hence, a sensitivity study of variables controlling the fluid flow in fractures was carried out by means of parametric runs. In these parametric run fracture orientation, fracture spacing, and injection rate were varied and the flow pattern that resulted were recorded.

It was observed that smaller fracture spacing gave large pore pressure increments. A fracture orientation affects the effective normal stress acting on the fractures. This in turn determines the pore pressure distribution in fracture network. Pore pressure changes are smallest when effective normal stress of fracture in equal to principal normal stress in plane of fracture. Higher injection rate pumps more fluid into the fracture. The pore pressure increased approximately by 50 % when injection rate was doubled.

In low permeability gas reservoirs, a hydraulic fracture shows a huge impact on recovery of the gas. The recovery is increased over 50% with the presence of hydraulic fracture. The recovery of gas depends on fracture permeability and matrix permeability.

Doubling of fracture permeability gave a gain of approximately 20 % of gas recovery. In tight gas formations rock matrix has inherently lower permeability than a

conventional gas reservoir. When rock permeability was increased by factor of 2, the gas recovery did not change significantly.

Permeability of fracture dominates gas production from tight gas sands. Any increase in permeability either by introducing new fractures or by stimulation of existing fractures opens new means of increasing the gas recovery. Since matrix is inherently less permeable, the gas recovery is significantly improved by smaller changes in fracture permeabilities. Hydraulic fracturing is promising in increasing the gas recovery from tight gas systems where stimulation of natural fractures is difficult and/or uneconomical.

CHAPTER 7

FUTURE WORK

A fully coupled simulation including geomechanics and fluid flow in reservoir simulator is recommended. The UFES simulator can establish the capability of various numerical methods like CVFEM, FEM and include this fully coupled approach. Currently, only fracture flow was analyzed and inclusion of the matrix flow should be considered.

More detailed sensitivity analyses with larger domain and fracture network can be carried out. A better computational technique should be implemented to speed up the simulation and hence reduce computational expense.

Additional studies can be done for the shale gas reservoir and coalbed methane. Currently UFES simulator lacks the module for investigation of shale gas reservoir or coal bed methane. This additional module should have the capability of considering the adsorption, desorption terms to the UFES simulator. This will be a valuable add-on and can help in carrying out other tight gas reservoir studies.

APPENDIX

FUNDAMENTALS RESERVOIR PROPERTIES

A Reservoir fluid properties

A-1Formation value Factor

A-.2 Gas-Oil Ratio

A-3 Fluid Saturation

Some of the important fluid, rock and geomechanical properties are discussed in detail.

A Reservoir fluid properties (Ahmed, 2006)

A-1 Formation Value Factor

Formation volume factor for a reservoir fluid is defined as the volume of the reservoir oil required to produce one barrel of oil in the stock-tank. Since the reservoir oil includes dissolved gas, the units are barrels of fluid at reservoir conditions per barrel of stock-tank fluid, res bbl/STB. The volume of stock-tank oil is always reported at 60°F.The formation factors of gas phase are expressed by the equation A- 1.1

GAS:

$$B_g(P_g) = \frac{[V_g]_{RC}}{[V_g]_{stc}} = \frac{\rho_{g,STC}}{\rho_{g,RC}} \qquad \text{(A-1.1)}$$

The reservoir fluids are classified into five different types: black oil, volatile oil, retrograde gas, wet gas, and dry gas. The five types of reservoir fluids have been defined because each requires different approaches by reservoir engineers and production engineers.

A-2 Solution Gas-Oil Ratio

The solution gas-oil ratio describes the mass transfer between the oil and gas phases for a multiphase problem. The quantity of gas dissolved in oil at reservoir conditions is called the solution gas-oil ratio. The solution gas-oil ratio is also the amount of gas that is evolved from the oil as the oil is transported from the reservoir to surface conditions. This ratio is defined in terms of quantities of gas and oil which appear at the surface during production and is given by equation (A-1.2)

$$R_s = \frac{\rho_{g,STC}}{\rho_{g,RC}} \tag{A-1.2}$$

The surface volumes of both gas and liquid are referred to standard conditions, so that the units are standard cubic feet per stock-tank barrel, scf/STB. The solution gas-oil ratio is also called dissolved gas-oil ratio and occasionally gas solubility.

A-3 Fluid Saturation

There can be multiple fluids, i.e., oil, water, and gas in the rock pore for multiphase flow. Fluid saturation S_l, is defined as fraction of pore volume occupied by any fluid phase. Therefore, in the water and gas flow problems the saturations must obey

the equation A-1.3., whereas in oil, water, and gas flow problems the saturations must obey the equation A-14.

$$Swater + Sgas = 1. \quad \text{(A-1.3)}$$

$$Soil + Swater + Sgas = 1. \quad \text{(A-1.4)}$$

B. Rock Properties

B-1 Porosity

Porosity is the first essential attribute of a reservoir. The porosity of a medium is the void space inside the medium that can be occupied by fluids like oil, water, and gas. Porosity, φ, is either expressed as the void ratio, which is the ratio of voids to the ratio of solid rock, or more frequently as a percentage given by

$$\phi = \frac{V_{void}}{V_{total}} \quad \text{(B-1.1)}$$

where Vvoid is the volume of the rock pore and Vtotal is the total volume of the rock.

B-2 Permeability

Permeability is the second essential attribute for a reservoir rock. Porosity alone is not enough, the pores must be connected. Darcy's law used to calculate fluid flow rate from the pressure gradient in the case of single-phase flow is given by

$$v = -\frac{k}{\mu}(\Delta P + \frac{g}{g_c}) \qquad \text{(B-1.2)}$$

where k is the absolute permeability tensor of the porous media,

μ is the viscosity of the fluid,

∇P the pressure gradient and g is the gravity vector.

The permeability tensor in three-dimensional space is given by

$$\text{k} = \begin{bmatrix} kxx & kxy & kxz \\ kyx & kyy & kyz \\ kzx & kzy & kzz \end{bmatrix} \qquad \text{(B-1.3)}$$

In most practical problems, it is possible or necessary to assume that k is a diagonal tensor given by kx, ky and kz. If kx = ky = kz, the medium is called isotropic, otherwise anisotropic.

B-3 Relative Permeability

The absolute permeability defined in section A-1.2.2 represents the permeability of the entire phase in single phase flow. To account for the simultaneous flow of multiple phases, i.e., oil, water, and gas, a rock property, relative permeability, is introduced into Darcy's law. Therefore, Darcy's law for multiphase flow is

$$v = -\frac{kk_{rl}}{\mu_l}(\Delta P + \frac{g}{g_c})$$

The relative permeability krl, of a particular phase is a function of the phase saturation, Sl. Water and gas phase relative permeabilities are typically functions of water

and gas saturations, respectively, but oil phase relative permeability in a three-phase system is estimated from two sets two-phase data: relative permeability

in an oil-water system

$$krow = f(Sw) \tag{B-1.4}$$

and in an oil-gas system

$$krog = f(Sg) \tag{B-1.5}$$

C Geomechanical Properties

C-1 Bulk Modulus

Bulk modulus (*k*) is the ratio of the confining pressure to the fractional reduction of volume in response to the applied hydrostatic pressure. The volume strain is the change in volume of the sample divided by the original volume.

Bulk modulus is also termed the modulus of incompressibility.

The bulk modulus K can be formally defined by the equation:

$$K = -\frac{V\partial P}{\partial V} \tag{C-1.1}$$

where P is pressure, V is volume, and ∂P/∂V denotes the partial derivative of pressure with respect to volume. The inverse of the bulk modulus gives a material's compressibility. Other moduli describe the material's response (strain) to other kinds of

stress: the shear modulus describes the response to shear, and Young's modulus describes the response to linear strain. For a fluid, only the bulk modulus is meaningful.

C-2 Shear Modulus

Shear modulus, G, is the ratio of the shear strain to the applied shear stress. It is a measure of the sample's resistance against deformation. The shear modulus is given as

$$G = \left(\frac{F/A}{\Delta x/l}\right) = \left(\frac{F}{A\Delta x}\right) \qquad \text{(C-1.2)}$$

Shear modulus is usually expressed in gigapascals (GPa) or thousands of pounds per square inch (psi).

C-3 Young Modulus

Young's modulus, E, is the ratio of longitudinal stress to longitudinal strain. It can be interpreted as the rock stiffness (the resistance of the rock to deform under a given loading condition). The equation relating the Young's modulus to Poisson's ratio and the shear modulus is given as

$$E = 2.G/ (1+\upsilon) \qquad \text{(C-1.3)}$$

C-4 Permeability Modulus

To study fluid flow through stress dependent porous media, a new parameter (Ahmed, McKinney), the permeability modulus orΥ. is defined

$$\nu = -\frac{1.\mathrm{dk}}{\mathrm{K.d}p} \qquad \text{(C-1.4))}$$

This parameter plays a very important role in systems where changes in effective stress affect permeability. Basically, it measures the dependence of hydraulic permeability on pore pressure. For practical purposes, the permeability modulus is assumed constant. Thus, permeability varies exponentially with pore pressure.

$$k = k_i e^{-\gamma(p_i - p)} \qquad \text{(C-1.5)}$$

In view of the similar appearance of permeability and density in the diffusion equation, it may be advantageous to assume an exponential relationship between permeability and pressure.

C-5 Poisson's Ratio

Poisson's ratio (v) is the ratio of lateral strain (perpendicular to an applied stress) to the longitudinal strain (parallel to applied stress) when a longitudinal strain is applied.

$$\nu = -\frac{\mathrm{d}\varepsilon_{lateral}}{\mathrm{d}\varepsilon_{longitudinal}} \qquad \text{(C-1.5)}$$

$\varepsilon_{lateral}$ and $\varepsilon_{longitudinal}$ are lateral and longitudinal strains, respectively.

REFERENCES

Addis, M.A., and Yassir ,N., 2010, An Overview of Geomechanical Engineering Aspects of Tight Gas Sand Developments, SPE/DGS Saudi Arabia Section Technical Symposium and Exhibition, 4-7 April 2010, Al-Khobar, Saudi Arabia

Ahmed T., 2002. Reservoir Engineering Handbook, Second edition, Gulf Professional Publishing

Ahmed, T., and McKinney P., 2004. Advanced Reservoir Engineering, Gulf professional publishing

Aziz, K., and Setteri, A., 1979. Petroleum Reservoir Simulation, New York: Elsevier Applied Science Publishers, 1979

Barton, N. R., Bandis, S. C., and Bakhtar, K., 1985. Strength, deformation and conductivity coupling of rock joints, Int. J. Rock Mech. Min. Sci. 121-140 1985

Cundall, P. A. 1988. Formulation of a three-dimensional distinct element model—part i. a scheme to detect and represent contacts in a system composed of many polyhedral blocks, Int J. Rock Mech. Min. Sci. & Geomech, 25(3), 107-116 1988

Dicman, A., Putra, E., and Schechter, D., 2004 Texas A&M University, Modeling fluid flow through single fractures using experimental, stochastic and simulation approaches, SPE/DOE Symposium on Improved Oil Recovery, 17-21 April 2004, Tulsa, Oklahoma

Jolly, R.J.H,,Wei L., and Pine, R.J. 2000. Stress sensitive fracture flow modeling in fracture reservoirs, SPE International Petroleum Conference and Exhibition in Mexico, 1-3 February 2000, Villahermosa, Mexico

Longuemare, P., Mainguy1, M., Lemonnier, A., Onaisi, Ch., and Koutsabeloulis N., 2002. Geomechanics in Reservoir Simulation: Overview of Coupling Methods and Field Case Study, Oil & Gas Science and Technology – Rev. IFP, Vol. 57 2002, No. 5, pp. 471-483

Lorenz, J.C., 1999. Stress-sensitive reservoirs, Journal of Petroleum Technology Volume 41, Number 6 June 1989 Pp 615-622

Manual Itasca, 2007 .3DEC version 4.2.10.64, 2007, Itasca consulting group,Inc

Mas Ivars, D. 2006 "Water Inflow Into Excavations in Fractured Rock -- A three-dimensional hydro-mechanical numerical study," Int. J. Rock Mech. Min. Sci., 43, Pp 705-725

Min, K., Rutqvist, J., Tsang, C., and Jing, L., 2004 Stress-dependent permeability of fractured rock masses: a numerical study Int. J. Rock Mech. Min. Sci 41 2004 Pp1191–1210

Moridis, G., Blasingame , T.A., and Freeman C.M. 2009. Analysis of mechanism of flow in tight gas and shale gas reservoirs, SPE Annual Technical Conference and Exhibition, 4-7 October 2009, New Orleans, Louisiana

Nur, A.,and Yilmaz, O., 1985. Pore Pressure Fronts in Fractured Rock Systems. Department of Geophysics Stanford University, Stanford, CA

Osorio, J.G., SPE, and Lopez, C.F. 2009. Geomechanical factors affecting the hydraulic fracturing performance in a geomechanically complex, tectonically active area in Colombia. Latin American and Caribbean Petroleum Engineering Conference, 31 May-3 June 2009, Cartagena de indias, Colombia

Osorio, Jose G, Chen, Her-Yuan., Teufel, Lawrence W., and Schaffer, S., 1997. Numerical simulation of coupled fluid-flow/geomechanical behavior of tight gas reservoirs with stress sensitive permeability, Latin American and Caribbean Petroleum Engineering Conference, 30 August-3 September 1997, Rio de Janeiro, Brazil

Samier, P., Onaisi, A., and Fontaine, G., 2003. Coupled analysis of geomechanics and fluid flow in reservoir simulation, SPE Reservoir Simulation Symposium, 3-5 February 2003, Houston, Texas

Schildt, H., 1999. C++: The Complete Reference, third ed. New York: McGraw-Hill, 1999

Tran, D., Nghiem L., and Buchanan L., 2005. SPE, Computer Modeling Group Ltd, An overview of iterative coupling between geomechanical deformation and reservoir flow, SPE/PS-CIM/CHOA International Thermal Operations and Heavy Oil Symposium, 1-3 November 2005, Calgary, Alberta, Canada

Warpinski, N.R., Mayerhofer, M.J., Vincent, M.C., Cipolla, C.L., and Lolon, E.P., 2008. Stimulating Unconventional Reservoirs: Maximizing Network Growth While Optimizing Fracture Conductivity, SPE Unconventional Reservoirs Conference, 10-12 February 2008, Keystone, Colorado, USA

Whittaker, B. N., Singh, R. N., and Sun, G., 1992, Rock fracture mechanics, principles, design and applications, developments in geotechnical engineering, 71, Elsevier, Amsterdam

Witherspoon, P. A.,.Wang, J. S.,Iwai K., and J. E. Gale., 1980. Validity of cubic law for fluid flow in a deformable rock fracture, Water Resources Res., 16(6), 1016-1024 1980

Yang, Y., 2003. Finite element multiphase flow simulation, Thesis, University of Utah